On the Suspension of Graded Sediment by Waves above Ripples : inferences of convective and diffusive processes

A.G Davies[a,*] and P.D Thorne[b]

[a] Centre for Applied Marine Sciences, School of Ocean Sciences, Bangor University, Menai Bridge, Anglesey LL59 5AB U.K.

[*] Corresponding author: Email: a.g.davies@bangor.ac.uk; Tel +44 (0)1248 383933

[b] National Oceanography Centre, Proudman Building, 6 Brownlow Street, Liverpool L3 5DA U.K. Email: pdt@noc.ac.uk

Abstract

The relationship between the grain size distribution of the sediment on the bed and that found in suspension due to wave action above ripples is assessed here using detailed, pumped sample, measurements obtained at full-scale and also at laboratory scale. The waves were regular and weakly asymmetrical in most tests, and irregular in a minority of tests. The beds comprised fine and medium sand and were rippled in all tests. The cycle-mean sediment concentrations (C) from the pumped samples were split into multiple grain size fractions and then represented by exponential C-profile shapes. The analysis of these profiles was carried out in two stages to determine: i) the relationship between the size distribution of the sediment on the bed and that found in the reference concentration, and ii) the behaviour of the exponential decay scale of the C-profiles. From this analysis inferences are made about the relative roles of diffusion and convection in the upward sediment flux linked to the process of vortex shedding from the ripple crests. The Transfer Function (Tr) defined to relate the bed sediment size distribution to that of the reference concentration indicates that, while finer fractions are relatively easily entrained, the suspension of some coarser fractions is caused by an additional convective effect that supplements diffusion. The evidence for this becomes pronounced above steep ripples, and the Transfer function suggests further that irregular waves increase the occurrence of coarser fractions in suspension. A functional form for Tr is suggested incorporating these principles. The exponential decay scale L_S arising from the fractional C-profiles is also examined to assess the mechanisms responsible for the upward transfer of grains and a parameterisation of L_S related to ripple size is suggested. The separate findings for Tr and L_S present supporting evidence of diffusion affecting the finer fractions in suspension and combined diffusion + convection affecting the coarser fractions. The methodology developed allows the vertical profile of suspended median grain size to be predicted given knowledge of both the bed grain size distribution and also the flow conditions.

Keywords: Sediment transport; Waves; Graded sediment; Sand ripples; Reference concentration; Suspended concentration profiles.

List of symbols

a	coefficient in Eq. (A.2)
a_1,a_2	coefficients in ripple 'flow contraction' expression
A_1	semi-orbital near-bed excursion amplitude based on the wave fundamental frequency
A_*	($=D_*^3$) Archimedes Buoyancy Index
b	coefficient in Eq. (A.2)
b_1,b_2	coefficients in Transfer function expression (Eq. (14))
B_1,B_2	dimensional coefficients with numerical values depending upon ν, s and g
c_1-c_4	empirical constants
C	wave cycle-mean sediment concentration
C_0,C_a,C_r	sediment volumetric reference concentration at height z = 0, z=a and z=z_r , respectively.
C_{bi}	bed sediment volumetric concentration of the i^{th} grain fraction
C_{ri}	volumetric reference concentration of the i^{th} grain fraction (< … > denotes a wave cycle-mean)
C_{cb}	cumulative %-distribution of bed sediment sizes
C_{cr}	cumulative %-distribution of reference concentration particle sizes
$C_i(z_j)$	suspended concentration of the i^{th} grain fraction at the j^{th} height z above the bed
$C_{cum,i}(z_j)$	cumulative concentration based on $C_i(z_j)$
$C_{sum}(z_j)$	total concentration summed over the i grain fractions at the j^{th} height z above the bed
d	sediment grain size; this includes sizes obtained by interpolating the discrete d_m scale
d_c	maximum allowable or critical grain size in suspension
d_s	sieve size used in grain distribution analysis
d_m	grain size corresponding to central diameter for each sieve interval determined at the respective mid-points on the ϕ scale
d_{50}	median grain diameter of the sediment
d_{50b}	median grain diameter of the bed material
d_{50s}	median grain diameter of the sediment in suspension
d_i	sediment grain diameter (bed or suspended material) for which i% of the grains are finer by volume (or weight)
d_0	($=2A_1$) near-bed orbital diameter
D_*	dimensionless grain size (defined by Eq. (10))
f_w	wave friction factor ($f_{w,max}$ is maximum value according to Swart's (1976) formula)
g	acceleration due to gravity
H, H_s	wave height, significant wave height

k_s equivalent bed roughness

L_S ($=\varepsilon_s/w_s$) decay (or distribution) length scale of the exponential C-profile

L_{ST} total decay (or distribution) length scale for the aggregated C-profile

Re_s Reynolds number of a settling grain ($=w_s d/\nu$),

RE wave Reynolds number ($=U_1 A_1/\nu$)

s ($=\rho_s/\rho$) relative sediment density

T, T_p wave period, peak wave period

Tr 'Transfer function' relating the reference concentration to the bed sediment

u_* friction (or shear) velocity (with prime u_*' : skin friction component)

u_{*w} peak value of friction (or shear) velocity during the wave cycle (with prime u_{*w}' : as above)

U_1, U_2 first and second harmonics of the near-bed wave velocity amplitude

w upward fluid velocity (convective velocity in Fredsøe and Deigaard's (1992) model)

w_s sediment settling velocity

w_{sc} settling velocity corresponding to the critical grain size in suspension d_c

X non-dimensionalisation of grain diameter, defined by Eq. (14)

z height above the bed

z_a reference height above the bed at which $C = C_a$

z_r height of reference concentration C_r

β ($=\varepsilon_s/\varepsilon_m$) quotient describing the local difference between the diffusion of a fluid 'particle' and a discrete sediment particle

δ_s near-bed layer thickness in which sediment diffusivity ε_s remains constant

ε_e estimated sediment diffusivity in Fredsøe and Deigaard's (1992) convective model

ε_m eddy viscosity, or vertical diffusion coefficient for momentum, in a clear fluid

ε_s sediment vertical diffusivity

ϕ ($=-\log_2(d)$ with d in mm) Krumbein phi scale

η ripple height

λ ripple wavelength

ν kinematic viscosity of water

θ Shields parameter, peak value during wave cycle (Eq.(12) (with prime θ' : skin friction component)

ρ density of water

ρ_s density of sediment

σ_g $(=(d_{84}/d_{16})^{0.5})$ geometric standard deviation of the sediment

τ_b bed shear stress (< … > denotes a wave cycle-mean)

$\tau_{crit,i}$ critical shear stress for the i^{th} grain fraction of the bed sediment in isolation

τ_e time scale of exchange in Fredsøe and Deigaard's (1992) convective model

ω ($=2\pi/T$) wave angular frequency

1. Introduction

Although the seabed sediment typically comprises a broad size distribution surprisingly little account is taken of this in many of the methods used in sediment transport estimation. A single representative grain size is generally used to characterise the sediment even though the seabed includes both fine grain fractions that can readily be entrained into suspension, for example by waves, and also coarse fractions that only ever form part of the bed load. The resulting grain size distribution in suspension can be significantly different from that of the seabed. Further, due to the larger settling velocities of the coarser fractions, the suspended sediment size distribution becomes progressively dominated by finer grains as height above the bed increases. This has significant implications, for example in relation to sediment sorting across beach profiles and to water quality where contaminants are attached to finer or coarser particles. If the vertical sorting of sediment grains between the bed surface material and the suspension, and hence the relative movement of finer and coarser particles, is not taken into account, this may lead to bias and inaccuracy in predicting net sediment transport rates. In a series of laboratory experiments involving different sand mixtures beneath asymmetric waves, O'Donoghue and Wright (1994) showed that the relative contributions to the net transport, in suspension and in the near-bed sheet flow layer, varied significantly depending upon the sand size and grading.

Detailed procedures for modelling grain mixtures have remained rather *ad hoc*, with observations suggesting that some grain size fractions in suspension can be far coarser than accounted for by standard methodologies. For example, Masselink et al. (2007) estimated the sediment size in suspension above oscillatory ripples at a coarse-grained beach site to be 0.6mm with settling velocity 80 mm/s; these values are far larger than would be predicted by the turbulent diffusion methodologies referred to later. This raises the interesting and important question: 'Are all grain fractions in suspension in a given flow influenced in the near-seabed layer by the same mixing mechanisms?' The answer is implicit in some previous works (e.g. Van Rijn, 1993), but we return to the question here with the benefit of an extensive, detailed data set highlighting the suspension of graded sediments by waves above rippled beds. While arguing that the answer is 'No', we infer from the experimental data that, while the finer fractions in suspension are influenced primarily by diffusion, the coarser fractions are progressively influenced also by convection. The present study is in two parts, each involving suspended sediment data obtained beneath waves in both a full-scale wave facility and also a laboratory flume. Initially we consider the relationship between the size distribution of the sediment on the bed and that in suspension, and then the nature and causes of

the concentration profiles of the individual fractions in suspension. A similar study was carried out for steady flow by Sengupta (1979) who related the size distribution of the bed material to that obtained in suspension by pumped sampling at a fixed height above the bed. While Sengupta produced results analogous to some of those presented in this paper, the nature of his observations precluded discussion of the causes of the suspensions studied, which is a central aim here.

2. Background

2.1 Selective entrainment of graded sediment

Non-uniformity of the bed material results in selective entrainment processes commonly represented by a hiding and exposure correction to the critical shear stress for the threshold of motion (e.g., Egiazaroff, 1965). This increases the critical stress for finer particles and decreases it for more exposed coarser particles (Wiberg and Smith, 1987; Van Rijn, 1993; Wallbridge et al., 1999; Hassan 2003). In a multi-fraction approach Van Rijn (2007b) included an additional correction to the shear stress itself due to Day (1980). The suspended concentration (C) can then be determined using reference concentrations for the individual size fractions in the bed (Wallbridge and Voulgaris, 1997). Sistermans (2002) found, however, that for wave + current flows above rippled beds it was not possible to predict near-bed reference concentrations per fraction satisfactorily using hiding and exposure concepts, due to the sensitivity of such calculations and also lack of understanding of the processes. Nielsen (1992), while noting that there was little information available about the selective entrainment of different sand sizes under waves, proposed a simple 'rule of thumb' to relate the sediment in the bed to that found in near-bed suspension (see §5 and Appendix B). The uncertainties arising from Nielsen's (1992) approach, together with the findings of Sistermans (2002) and Hassan (2003) pointing to the difficulties in understanding selective entrainment processes, have motivated here a different approach based on a 'Transfer Function' that links the sediment on the bed to that in the flow.

The relationship between the suspended median grain size d_{50s} and that of the bed material d_{50b} depends upon the degree of non-uniformity of the bed sediment expressed, for example, by the quotient d_{90}/d_{10}. Based on experiments with irregular waves Van Rijn (2007b) noted that for relatively 'uniform' bed sediment having d_{90}/d_{10} = 1.8-2.1 the quotient d_{50s}/d_{50b} was in the range 0.7-0.9, while for less uniform 'graded' material having $d_{90}/d_{10} \approx 4.7$ the range was 0.35-0.45. Similar conclusions were reached by Sistermans (2002). In both the rippled regime (Sistermans, 2002), and

also the oscillatory sheet-flow regime (Hassan, 2003), the suspended median size d_{50s} has been found to become smaller with increasing height above the bed.

2.2 Mixing in the wave boundary layer

Although the C-profiles investigated in this paper are wave cycle-averaged, their origin lies in the intra-wave mixing processes in the wave boundary layer. These processes are fundamentally different above plane and rippled beds formed, respectively, in oscillatory flows by waves having large and small height. Above *plane* beds momentum transfer occurs primarily by turbulent *diffusion*, whereas above steeply *rippled* beds momentum transfer and the associated sediment dynamics are dominated by coherent, periodic vortex structures (Davies and Thorne, 2008). These vortices are shed from the ripple crests at each flow reversal and dominate the near-bed dynamics in a *convective* layer of thickness 1-2 ripple heights. Above this the coherent motions break down to be replaced by random turbulence, with the overall effect that sand is entrained to considerably greater heights above rippled beds than above plane beds.

Even above steeply rippled beds, the conceptual basis for the interpretation of (vertical) C-profiles is normally taken as being turbulent diffusion. If temporal and also (horizontal) spatial variations in such profiles are neglected, the balance between upward diffusion and downward settling is expressed through the 1D-vertical (1DV) advection-diffusion equation:

$$\varepsilon_s \frac{dC}{dz} + w_s C = 0 \tag{1}$$

where C is the wave-averaged concentration at height z above the bed, ε_s is the sediment diffusivity and w_s is the settling velocity. The sediment diffusivity is then usually related to the diffusion coefficient for momentum, or eddy viscosity, for a clear fluid (ε_m), as follows:

$$\varepsilon_s = \beta \varepsilon_m \tag{2}$$

where for relatively low sediment concentrations the 'damping' of turbulence by suspended sediment can be ignored (Li and Davies, 2001), and where the β-factor then describes the difference between the diffusion of a fluid 'particle' and a discrete sediment particle. It is not obvious that the gradient diffusion assumption used in Eq. (1) should have any relevance in the oscillatory boundary layer above ripples since the 'free paths' of the larger eddies responsible for momentum transfer are not, in general, 'small' compared with the size of the mixing domain. This difficulty has been addressed by Nielsen and Teakle (2004), while the basis of a diffusive modelling approach has been considered by Davies and Villaret (1997) and Malarkey and Davies (2004). In practice, the relationship between ε_m and ε_s may be more complicated than Eq. (2) suggests, with some finer

fractions in suspension being represented by this equation quite well, but other coarser fractions far less well.

As far as the vertical structure of ε_m above rippled beds in oscillatory flow is concerned, Davies and Villaret (1997) found, for very rough turbulent flows having $A_1/k_s<5$, that in a layer of approximate thickness 2η, where η is the ripple height, ε_m is well represented by Nielsen's (1992) height-invariant, wave-averaged, expression for very rough beds, given by:

$$\varepsilon_m = c_1 A_1 \omega k_s \tag{3}$$

where A_1 is the semi-orbital excursion amplitude near the bed, ω (= $2\pi/T$) is the wave angular frequency (T = wave period), and the empirical constant c_1 =0.004, with k_s the equivalent bed roughness, given by:

$$k_s = 25\eta\left(\eta/\lambda\right) \tag{4}$$

where λ is the ripple wavelength. A similar height-invariant formula for ε_m was proposed by Sleath (1991). The dynamical significance of eddy shedding is expected to become pronounced when $\eta/\lambda \geq 0.1$. In this case the solution of Eq. (1) for the suspended concentration becomes simply:

$$C = C_0 e^{-z/L_s} \tag{5}$$

where L_S (=ε_s/w_s) is the decay (or distribution) length scale, C_0 is the wave-averaged 'reference' concentration at height z=0, with the β-factor in Eq.(2) treated as a constant for a particular grain size in suspension. For rippled beds in oscillatory flow, the cause of the 'β-effect' has been analysed by Malarkey et al. (2015); Nielsen (1992) suggested that β is equal to about 4, a value found appropriate by Thorne et al. (2002) and Davies and Thorne (2005).

The β-effect has been found to occur also above 'dynamically plane' beds comprising ripples of low steepness which induce less vortex shedding. Above such beds the mixing length scale is normally assumed to increase with height and the eddy viscosity is taken in the form

$$\varepsilon_m = c_2 u_* z \tag{6}$$

where u_* is an appropriate shear velocity and c_2 is a constant. In this case the solution of Eq. (1), subject again to Eq. (2), becomes

$$C = C_a\left(z_a/z\right)^{w_s/c_2\beta u_*} \tag{7}$$

where C_a is the reference concentration at height $z=z_a$. Sistermans (2002) tested 10 different functional forms for the vertical profile of the sediment diffusivity ε_s, including Eqs. (3) and (6), and concluded that, for irregular waves + current above a rippled bed, turbulent diffusion can describe the C-profiles and also the d_{50s} profile if size grading is taken into account (see Appendix A). In the

experiments referred to in §2.1, Sistermans (2002) noted that higher suspended concentrations occurred for 'graded' sediment than for more 'uniform' sediment, but with the respective near-bed reference concentrations being approximately equal. The implied ε_s value was somewhat larger (by ~10%) for the graded sediment in these tests.

Above dynamically plane beds in steady flow, Van Rijn (1984) analysed C-profiles measured by Coleman (1981) and obtained the expression:

$$\beta = 1 + 2\left({}^{w_s}/_{u_*}\right)^2 \qquad for \qquad 0.1 < {}^{w_s}/_{u_*} < 1 \tag{8}$$

According to Eq. (8), the increase in the effective sediment diffusivity is greater for relatively larger (i.e. faster settling) particles in suspension. Van Rijn suggested that this this was due to the increasing influence of centrifugal forces even in steady cases where eddy shedding from the bed is less well organised than in oscillatory flows. However Sistermans (2002) reanalysed Coleman's data and could not find any dependence of β on the suspended sediment size. Nevertheless Van Rijn (2007a) incorporated Eq.(8) in his more recent formulation for wave and current flows.

In practice, very few formulations for ε_s have taken account of the β-effect. A notable exception was that of Van Rijn (1989) (see Van Rijn, 1993) for unsteady flow based on ε_s being height-invariant in a near-bed layer of thickness δ_s. Above rippled beds, δ_s was taken equal to 3η implying shed-eddy sizes that scale on the ripple height. Van Rijn's (1989) formula for ε_s utilises Eqs. (2) and (3), with k_s taken equal to δ_s and, importantly, with β effectively taken equal to the dimensionless grain size D_* as follows:

$$\varepsilon_s = c_1 D_* A_1 \omega \delta_s \tag{9}$$

where

$$D_* = d\left({}^{(s-1)g}/_{\nu^2}\right)^{1/3} \tag{10}$$

with $s=\rho_s/\rho$ (ρ_s = sediment density, ρ= water density), g = acceleration due to gravity, and ν = kinematic viscosity of water. So again the greater is the grain size d in suspension the greater is ε_s according to Eq. (9), the D_* parameter expressing the increased mixing observed for larger particles. Van Rijn's (2007a) more recent expression for ε_s has the same general height-constant nature as Eq. (9) in the near-bed layer, but with $c_1 D_*$ replaced by 0.018β (wherein the peak value u_{*w} during the wave cycle is used in Eq. (8)) and with δ_s replaced by $2\delta_w$ where δ_w is the thickness of the wave boundary layer (see Van Rijn (2007a) for the details). This formulation also caps the value of β at 1.5

which limits the mixing of the larger suspended particles. Both of Van Rijn's formulations for ε_s are compared with the present data in §6.

2.3 Convection and diffusion in the wave boundary layer

The sediment mixing giving rise to the C-profile is linked to the other main issue addressed here, namely the relationship between the sediment size distribution on the bed and that in suspension. A commonly used criterion to determine whether or not a sediment grain will be entrained is that of Fredsøe and Deigaard (1992). They suggested that a particle should be able to remain in suspension provided that its settling velocity (w_s) is sufficiently small compared with the near-bed vertical turbulent velocity fluctuations, the magnitude of which are of the order of the (skin friction) shear velocity u_*'. Davies and Thorne (2002) used this criterion to define the maximum allowable, or critical, grain size in suspension (diameter = d_c) to be that having settling velocity $w_{sc} = 0.8\, u_{*w}'$ where u_{*w}' is the peak wave-induced skin-friction shear velocity. However, for the wave conditions studied, including some of the same experiments considered later, they found that this essentially diffusive approach failed to account fully for the rapid increase observed in d_{50s} on approaching the bed, caused by the presence of coarse fractions having size significantly larger than d_c.

The presence in suspension of grains having $d>d_c$ points to a mechanism other than turbulent diffusion to balance sediment settling. Fredsøe and Deigaard (1992) considered the effect of an upward convective flux of sediment arising from either vortex shedding above ripples in oscillatory flow or from coherent motions arising from the bursting process in steady flow. In their convection model, upward moving (with constant velocity w) parcels of sediment-laden fluid exchange water and sediment (with time scale of exchange τ_e) with the surroundings in which the concentration is assumed to be very much smaller than in the parcel itself. The parcel travels upwards with constant velocity exchanging fluid and sediment as it does so. The steady-state balance between settling in the surrounding fluid (with velocity w_s) and upward vertical convection gives rise to a mean concentration profile that decays exponentially with height. When this profile is *analysed* in order to determine the implied, estimated turbulent diffusion coefficient (ε_e) in equation (1) it turns out that $\varepsilon_e = w_s w \tau_e$ indicating an apparent diffusion coefficient that increases with the settling velocity. Treating w and τ_e as constants, Fredsøe and Deigaard's convection argument leads to the conclusion that ε_e/w_s = constant and, thus, that the relative suspended concentration will be the *same* for all grain sizes. Tomkins et al. (2003) observed this effect for regular waves above a rippled bed of mixed quartz and heavy mineral sand. The vertical gradients of the time-averaged suspended C-profiles were found to be similar for the light and heavy minerals, despite their settling velocities

differing by a factor of about 1.5, implying a convective rather than diffusive distribution mechanism, at least for the heavy particles. Fredsøe and Deigaard's model was not intended to be a quantitative description, but simply an illustration of the process of convection. The same comment can be made about the behavioural model of Nielsen (1992) in which the process of 'pure convection' leads again to the relative suspended concentration being the same for all grain sizes. All this evidence seems to point to the need for a quantitative approach including a convective element to represent the coarser fractions in suspension.

From a practical standpoint, a number of empirical expressions have been proposed for the length scale L_s. Some of these are implicit in expressions for ε_s such as that of Van Rijn (1989) for the near seabed layer (Eq.(9)) (see §8.4.4 in Van Rijn(1993) for a catalogue of expressions). Others have been presented more directly, the most well-known of these being that of Nielsen (1990, see also 1992), namely:

$$L_s = \begin{cases} 0.075\dfrac{A_1\omega}{w_s}\eta & for \quad \dfrac{A_1\omega}{w_s} < 18 \\ 1.4\eta & for \quad \dfrac{A_1\omega}{w_s} > 18 \end{cases} \qquad (11)$$

Here it is the *finer* particles having smaller w_s values that exhibit the same concentration profile (i.e. with decay scale that depends *only* on η), and *not* the *coarser* particles as would be expected from the earlier considerations. In the interpretation of the present data sets we return to Equations (9) and (11), therefore, to establish whether one or the other better describes the data being analysed.

2.4 Present study

In §3 the experimental data and methods are introduced. This data is primarily from a large-scale wave flume facility in which regular and irregular waves were generated, but it is accompanied for comparison by a small-scale laboratory data set of McFetridge and Nielsen (1985). In each case wave-averaged C-profiles have been obtained by pumped sampling and these samples have then been subdivided into grain fractions. In §4 the methods used to analyse the measured C-profiles are discussed, including the justification for an assumed exponential C-profile shape (c.f. Eq.(5)) rather than a power law profile (c.f. Eq.(7)). Then in §5, using reference concentrations at the bed level based on best fits involving Eq.(5), the relationship between the size distribution of the bed sediment and that of the reference concentration is quantified using a 'Transfer Function'. The nature of this function is explored with emphasis on the ripple dimensions, on the presence of *fine* or *medium* sized sand on the bed, and on the (ir)regularity of the surface waves. Here it is established also whether grain fractions were present in suspension having size $d>d_c$. Next, in §6, the

inference that convection might be playing a role in determining the C-profile shape is explored through an analysis of the decay length scale L_s to determine whether or not the diffusive approach breaks down for the coarser fractions. The methods developed in §5 and §6 are used in §7 to recover profiles of d_{50s}. Some of the wider implications of the results are then discussed in §8 and the conclusions are presented in §9.

3. Experiments and Observational Methods

3.1 Experiments in a full-scale wave flume

Detailed measurements of sediment in suspension above ripples were made during a series of campaigns in the Deltaflume of Delft Hydraulics, now Deltares (Williams et al., 1998). The large size of this flume (230 m long, 5 m wide and 7 m deep) allowed the wave and sediment transport phenomena to be studied at full scale. A wave generator at one end of the flume produced either regular or irregular waves that propagated over the sediment test bed before dissipating on a beach at the opposite end. Two series of experiments are considered from which specific tests have been subject to detailed sediment analysis, namely a set of 4 tests carried out above a bed of fine sand (median diameter d_{50}=0.162 mm, geometric standard deviation $\sigma_g=(d_{84}/d_{16})^{0.5}$=1.7), and a set of 6 tests above a bed of medium sand (d_{50}=0.329 mm, σ_g=1.55). The majority of the tests were carried out with regular, weakly asymmetric waves having heights, *H*, and periods, *T*, in the ranges 0.4-1.3 m and 4-6 s, respectively. In addition, irregular waves (JONSWAP spectrum) were generated in 1 test above the fine sand and 2 tests above the medium sand, having significant heights (H_s) and peak periods (T_p) in the ranges 0.7-1.1 m and 4.7-5.1 s. Table 1 provides a list of the wave conditions measured by two surface-following wave probes. The sediment beds of thickness 0.5 m and length 30 m were placed approximately half way along the flume, above which the water depth was 4.5 m. To establish equilibrium conditions for the hydrodynamics and sediment transport, the waves propagated over the bed for about 1 hour before data were recorded.

The measurements were made primarily using the instrumented tripod platform 'STABLE' (Sediment Transport And Boundary Layer Equipment). The main cluster of instruments on STABLE was directed towards the wave generator. This comprised a triple-frequency acoustic backscatter system (ABS), with associated pumped sampling, and electromagnetic current meters (ECMs) at three heights above the bed (0.30, 0.61 and 0.91 m). The ripples were measured using an acoustic ripple profiler (ARP). This system uses a radially rotating 2 MHz acoustic pencil beam to measure a 3 m profile along the bed. Measurements of ripple profiles were made approximately every 60 s during the

tests. Full details of the experimental set up and instrumentation were given by Thorne et al. (2002,2009), and the minimal impact that STABLE had on the flow and bed forms was discussed by Williams et al. (2003). The present analysis is concerned with (i) pumped sample data collected at 10 heights above the bed between 0.05 and 1.55 m, (ii) output from the ARP which gave detailed measurements of the bed morphology, (iii) hydrodynamic measurements from the wave gauges and ECMs and (iv) output from the ABS system, which was used here only to reference the bed location. The novel feature of the present paper is the pumped sample data which has not previously been analysed in detail.

Ripples formed on the bed with heights, η, and wavelengths, λ, in the respective ranges 0.01-0.07 m and 0.2-0.9 m for the fine sand, and 0.04-0.07 m and 0.28-0.51 m for the medium sand (see Table 1). The corresponding ripple steepness η/λ was <0.1 in the former cases and >0.1 in the latter. The method by which the ripple dimensions were determined from the ARP results is described in §4.2. The duration of each test was 1024 s, during which the ripples tended to migrate in the direction of wave propagation. This was reflected by slight asymmetry in the profile shapes particularly in the tests with regular waves.

The bed elevation was tracked during each test using the backscatter returns at the three ABS frequencies (1, 2 & 4 MHz). The nearest range of the bed from the ABS was considered to be the ripple 'crest' range. It was not always clear from the ABS time series that a ripple crest had, in fact, passed beneath a particular transducer since, in some tests, the bed forms migrated by less than a full wavelength. However, for this study this 'nearest' range has been treated as the crest of a ripple where z=0 (z = height above the crest level). The bed level itself was determined to an accuracy of $\pm$5 mm from a clearly defined echo in the ABS returns (Thorne et al., 2002).

Much of the analysis that follows rests on measurements of sediment concentration made by pumped sampling; here the procedures of Bosman et al. (1987) guided the sampling methodology. Samples of suspended sediment were obtained at 10 heights above the bed in the range 0.05 to 1.55 m using two arrays of intake nozzles (diameter 4mm) oriented at 90° to the wave orbital motion. Each nozzle was connected to a plastic pipe through which a mixture of water and sediment was drawn to the surface through a peristaltic pump. The resulting simultaneous water/sand mixture from each sampling position was collected in 10 litre buckets. Once full, the sediment was allowed to settle and the excess water was poured away. The pumped sampling duration was about 15 min, which corresponded typically to 180 wave cycles. All samples were sealed in plastic bags for

subsequent grain size and settling velocity analyses, and also for measurement of the suspended, wave-averaged, sediment concentration. Although pumped sample measurements were made in the nominal height range 0.05 to 1.5 m above the bed, size analysis was generally restricted to heights below ~0.5 m due to the reduced sediment mass collected above this. The grain size analyses reported here were carried out by a contractor using standard sieving techniques which, depending upon individual test conditions, resulted in the C-profiles being subdivided into up to 15 fractions with a ¼-ϕ increment ($\phi=-\log_2 d_s$ where d_s is the grain diameter corresponding to the sieve size in mm). The grain size distribution of the bed material was also determined by sieving bottom samples. Figure 1 shows the cumulative %-finer grain size distribution curves for the two sand sizes used in the Deltaflume, and also for the fine sand used in the laboratory experiment of McFetridge and Nielsen (1985) [hereafter MN85] described in §3.2.

3.2 Experiment in a small scale wave flume

For comparison with the 10 tests from the Deltaflume, a similar experiment carried out at small-scale by MN85 in a wave flume at the University of Florida is also considered. This provides both an independent assessment of the results from the Deltaflume and also some insight into whether any significant differences might occur between experiments carried out at full- and small-scale. The flume was 18.3 m long, 0.61 m wide and 0.91 m deep. Waves were generated by a piston-type wave maker at one end of the flume while a beach slope was present at the other end. Two series of tests were carried out, one with *natural* ripples, the other with *artificial* ripples (triangular strip roughness), though only the natural ripples are considered here. The hydrodynamic conditions (see Table 1) involved weakly asymmetrical waves of height 0.130 m and period 1.51 s in water of depth 0.30m. MN85 used stream function theory to estimate the peak forward and backward near-bed velocities as 0.278 and 0.216 m/s, respectively. Here this has been re-interpreted as being equivalent to a Stokes 2nd order wave having first and second harmonic velocity amplitudes of: U_1 = 0.247 m/s, U_2 = 0.031 m/s.

The sand bed was constructed in the central 3.15 m of the flume to a depth of 0.1 m. The bed comprised natural beach sand, but with the finer fractions augmented by the addition of quartz sand (~10% of the total). The resulting size distribution shown in Figure 1, while being similar to that of the fine sand used in the Deltaflume, departed from the classical lognormal distribution. MN85 quoted a mean grain diameter of 0.256 mm but, based on their cumulative grain size distribution, the analyses later in this paper have used: d_{50}=0.172 mm, σ_g=1.86. A multi-intake tube array was used to obtain a vertical profile of simultaneous, wave-averaged concentrations. The sampler array

was constructed of 3 mm diameter copper tubing with intakes having a vertical spacing of ~10 mm. Nine intakes oriented perpendicular to the flow were used to sample the ~0.09 m closest to the bed. Each pumped sample was divided into 6 grain size fractions with C-profiles presented for each fraction. MN85 analysed 240 pumped samples obtained during 5 repeated tests. The sand ripples during these tests were uniform and regular, with steepness significantly larger than the ripples in the fine sand in the Deltaflume (see Table 1).

4. Analysis of Waves, Ripples and Suspended Sediment Concentration Profiles

4.1 Near-bed velocity field and bed shear stress

It was found by Thorne et al. [2002] that, if linear wave theory is used to calculate the near-bed velocity amplitudes corresponding to the measured wave heights (*H*) and periods (*T*) given in Table 1, the results overestimate the amplitude of the first-harmonic (i.e. fundamental) component U_1 ($=A_1\omega$) measured by the ECMs on STABLE (at heights of 0.30, 0.61 and 0.91 m above the bed) by 9% $\pm$ 3%. Although this could have been due in part to the presence of STABLE itself, it is also the case that, since the waves were slightly asymmetric (i.e. weakly steep crested), linear theory may not provide a sufficiently accurate representation of the velocity field. In order to provide realistic inputs for the present calculations, a 9% reduction has been applied to the wave heights in Table 1 [following Thorne et al., 2002] and Stokes second-order theory has then been used to provide the near-bed values of U_1 and the amplitude of the second harmonic U_2 given in Table 2 (see Davies and Thorne (2005) for further explanation). Although this earlier procedure was developed for regular waves above the medium sand bed, including tests a8a, a11a, a20a & a21a, it has been extended here to both the fine sand and also irregular wave tests**.** The resulting near-bed asymmetry parameter ratio U_2/U_1 never exceeded 0.066, indicating the presence of weakly asymmetric waves. In the laboratory test of MN85 this ratio was somewhat larger (U_2/U_1 = 0.125).

Also listed in Table 2 for all tests are the corresponding values of: i) the near-bed orbital diameter ($d_0=2A_1$); ii) the critical (maximum) grain size (d_c) expected in suspension calculated using Fredsøe and Deigaard's criterion with $u_{*w}^{'} = \left(\frac{1}{2} f_w\right)^{1/2} U_1$ wherein the wave friction factor f_w has been determined using Jonsson's formula as expressed by Swart (1976) (Eq. (12)) and with w_{sc} given by Hallermeier's (1981) formulation for the settling velocity (Appendix C); iii) the Shields parameter (skin friction) given by

$$\theta' = {u'^2_{*w}}\Big/{(s-1)gd_{50b}} \quad , \quad f_w = exp\left[5.2\left(\frac{A_1}{2.5d_{50b}}\right)^{-0.19} - 6\right] \quad , \; f_{w,max} = 0.3 \quad ; \qquad (12)$$

iv) the wave Reynolds number RE (=U_1A_1/ν), v) the relative roughness A_1/k_s with k_s given by Eq. (4), and vi) the number of analysed grain fractions available for each test from the pumped sampling. Wiberg and Smith (1987) noted that, for mixed sediment beds, there are two length scales of importance: the diameter of the grain fraction of interest, and the local roughness scale of the surrounding bed which contributes to Eq. (12) through $k_s=2.5d_{50b}$.

For the Deltaflume tests, RE and A_1/k_s lie predominantly in the ranges (0.83-2.5)$\times10^5$ and (1.9-4.5), which correspond to the *very rough / rippled* regime (see the delineation of Davies and Villaret (1997), also Davies and Thorne (2008)). The test of MN85 (RE=0.11$\times10^5$, A_1/k_s=1.5) was carried out in the same turbulent flow regime.

4.2 Ripple dimensions

Figure 2 shows examples of ripple evolution measured using the ARP in the fine and medium sand during tests f5a and a8a. The ripples in the fine sand test, while being of somewhat larger wavelength than those in the medium sand (see Table 1) , were not only of smaller steepness, but were also less regular in shape with small secondary features occurring on the crests and also in the troughs of larger features. Some ripple migration occurred in the fine sand (Figure 2a), but this effect was more pronounced in the medium sand (Figure 2b).

To obtain the ripple height and wavelength, each ARP profile from the Deltaflume was processed and mean values obtained for the experiment as a whole (see Thorne et al. (2001) for details). Initially, each ripple profile was de-trended and given a zero mean. The ripple wavelength λ was then obtained from the zero crossing points which were averaged over the profile length. To estimate the ripple height η the absolute value of the zero-mean measured profile was taken, from which peaks were identified yielding the mean ripple height. The values of λ and η obtained for each profile were averaged to give the mean values listed in Table 1. Due to the complicated nature of the bed forms in some cases, this 'automated' method was checked by a direct visual interrogation of the ARP output. In the small-scale test of MN85 the ripple dimensions were determined by direct measurement through the glass side-wall of the flume.

The results in Tables 1 and 2 indicate that the quotient d_0/λ was in the range (1-1.7) for the fine sand and (1.8-2.3) for the medium sand tests in the Deltaflume, while d_0/λ was equal to about 1.5 for the

test of MN85. For the steeper ripples (η/λ>0.1) this suggests a more organised pattern of vortex shedding for MN85 than for the medium sand cases (see §6). Further, since the fine sand cases in the Deltaflume had η/λ<0.1, this might have been expected to limit the effectiveness of vortex shedding in the sediment entrainment process. Figure 3 shows the ripple dimensions in Table 1 scaled according to the prediction scheme of Wiberg and Harris (1994) which distinguishes between orbital, sub-orbital and anorbital ripples. This predictor is introduced here only to set the data within the familiar parameter ranges, rather than to imply its appropriateness. Following Davies and Thorne (2005, see Figure 7) the scheme has been modified by the application of a cap on the steepness η/λ of 0.14, which was found to be appropriate for the medium sand tests in the Deltaflume, some of which are repeated here, and which fell in the sub-orbital range. In addition Figure 3 includes the test of MN85 which falls in the middle of the orbital range and which is described well by the scheme. The fine sand cases from the Deltaflume exhibit longer wavelength and smaller steepness than predicted for sub-orbital ripples. However this behaviour has become well documented, as noted by Nelson et al. (2013). By continuing to increase in wavelength, but decrease in height and steepness, as d_0/d_{50b} increases these ripples can be categorized as 'long wave ripples' (see Soulsby, Whitehouse and Marten, 2012). Their effect on the measured C-profiles is explored in §6.

4.3 C-profiles and reference concentration

A significant step in the methodology concerns the choice made between fitting the measured C-profiles to an exponential profile (Eq.(5)) rather than a power law profile (Eq.(7)). In wave-induced flow, the former profile shape is usually expected to exist above a rippled bed while the latter is expected above a 'dynamically plane' bed. Here, as seen in Table 1, relatively steep ripples were found in the medium sand, while ripples of lower steepness were found for the fine sand (apart from the laboratory case of MN85). Furthermore each test involved multiple fractions of which some might have been better described by Eq.(5) and others by Eq.(7), or vice versa. Since the respective C-profile shapes are associated with height-invariant and linearly increasing sediment diffusivities, a generally applicable approach could involve a 'constant + linear' diffusivity profile (see Appendix A). However this has not been implemented here both due to the preponderance of exponential profile shapes in the pumped sample data, and also to preserve a basis for comparison with the previous literature.

For all of the tests carried out in the Deltaflume both exponential (log-linear) and power law (log-log) best fits were obtained for each grain fraction. Figure 4 shows the C-profiles obtained for the 14

fractions analysed for test a8a, together with the best fit exponential C-profile with 95% confidence limits included. The reference concentrations used in §5 were obtained from the intercepts at height z = 0, while the slopes provided the distribution length scales L_S used later in §6. For the tests with medium sand, the comparison between log-linear and log-log plotting indicated that an exponential fit was better for *all* of the smaller fractions analysed, while for some of the larger fractions a power law fit was just as good. For test a11a, an exponential fit was better for all fractions. In contrast, for the tests with fine sand the picture was less clear-cut; tests f5a and f8a were far better described by an exponential fit for all fractions, while test f7a seemed better described by a power law fit for all fractions. Test f3a was somewhere in-between, with an exponential fit being clearly better for all of the smaller fractions and for most fractions overall. Despite some uncertainty however, it has seemed well justified to proceed with the simplifying assumption that all fractions, in all tests, follow an exponential C-profile shape. An explanation as to why such a profile is particularly effective is suggested in Appendix A. MN85 took this approach also and the results quoted later are based on their best exponential fit outcomes for each of the 6 fractions analysed.

Figure 5 shows the reference concentrations obtained for the Deltaflume tests, with standard deviation error bars included. For each test two values are plotted against the Shields parameter (skin friction) θ' (see Table 2); the symbols $*$, x and • correspond to the sum of the concentrations obtained for the individual fractions, while the symbols □, O and ◊ correspond to the best fit obtained to the total aggregated C-profile. This latter fit produces a lower value of reference concentration for each test, apart from that of MN85 for which the two values are similar. [The reason for this difference is that, if two different exponential C-profiles are added, and a third exponential curve is fitted to the resulting convex, but not strictly exponential, shape, this best fit will have an intercept that is smaller than the notional reference concentration; see Figure 6 of Davies and Thorne (2002) for an illustration.] While the reference concentration in Figure 5 generally increases with increasing θ', it exhibits significant scatter, similar to that in the equivalent figure of Nielsen (1986, Fig. 2). The present paper is predicated on the existence of a sediment suspension, and does not treat the magnitude of the aggregated reference concentration any further (see Davies and Thorne (2005) for some further discussion). Instead the focus in what follows is the *relative* behaviour of the different grain fractions comprising the suspended load.

5. Reference concentration for grain fractions

The volumetric reference concentrations determined for the Deltaflume data are shown for four representative cases in Figure 6, each of which displays the same generally coherent behaviour. The grain size plotted on the horizontal axis denotes the central diameter d_m for each sieve interval determined at the respective mid-points on the ϕ scale (c.f. Figure 4), rather than the sieve ϕ-size d_s itself (c.f. Figure 1). Also shown are the reference concentrations determined at the crest level by MN85. For comparison with previous methods used to estimate fractional reference concentrations, each subplot includes predictions based on both Nielsen's (1992) near bed concentration (Eq. (B.1), see Appendix B) and also a formulation of the kind used by Wallbridge and Voulgaris (1997). This fractional, cycle-mean, reference concentration C_{ri} has been taken as proportional to $C_{bi}\left(\langle\tau_b\rangle - \tau_{crit,i}\right)/\tau_{crit,i}$ where C_{bi} is the volumetric bed concentration of the i^{th} fraction, $<\tau_b>$ is a representative mean bed shear stress which has been obtained from $<\theta'>=\theta'/\sqrt{2}$ and $\tau_{crit,i}$ is the critical shear stress derived from Shields curve for the i^{th} fraction in isolation with no hiding/exposure effects included. The calculations of $\tau_{crit,i}$ have been made using Soulsby's (1997) Eq. SC (77). Each of the dashed lines has been scaled such that its aggregated sum is equal to that of the observed reference concentration, and so only the patterns in Figure 6, and not the absolute values, have significance. The relationship between C_{ri} and C_{bi} is consistent in each subplot and the two fractional methods produce fairly similar results that agree best with the present observations for the medium sand. For the fine sand, the qualitative comparisons are less convincing, with the fractional approaches tending to follow the bed size distribution too closely. As shown in Appendix B, the resulting overestimation of the coarser fractions leads to a different outcome compared with the approach (Eq. (13)) proposed in what follows, which is based on the relationship between the cumulative grain size distributions for the reference concentration and the bed sediment.

To this end the fractional, measured, reference concentrations, c.f. Figure 6, have been expressed as a cumulative distribution for each test, as shown in Figures 7a and 7b in comparison with the distribution for the corresponding bed material. As expected the distribution curve for the reference concentration lies in every case to the left of that for the bed material, indicating the presence of generally finer material in suspension than is present on the bed, with the differences in the reference concentration curves reflecting the different test conditions.

In order to compare the reference concentration and bed sediment distributions, the 'raw' curves plotted in Figure 7 have been interpolated onto common grain diameter axes with an increment of 1 μm for the fine sand and 2 μm for the medium sand. This (spline-) interpolation was necessary due to the different bed and suspended grain size intervals in Figure 7. [This refined grain size scale,

based on interpolation of the discrete values d_m, is referred to hereafter by symbol d.] Thus it has been possible to define a continuous 'Transfer function' Tr relating the suspended sediment to the bed sediment by forming the quotient:

$$Tr = \frac{100 - C_{cr}}{100 - C_{cb}} \tag{13}$$

where C_{cr} and C_{cb} are the cumulative %-distributions for the reference concentration and bed sediment, respectively. The function Tr simply represents the broad trends in the relationship between the distributions shown in Figure 7, without recourse to hiding and exposure considerations for individual fractions. For grain sizes less than about 50 μm, for which data is sparse, the vagaries of the interpolation have been prevented from producing larger %-values for the bed sediment than for the reference concentration. It follows that the value of Tr is capped at unity for small grain sizes; as the grain size increases Tr then decreases indicating the successively lower level of transfer of bed particles into suspension. Figure 8 shows that the Transfer function has a consistent pattern in all tests and, as expected, there is a clear separation between the fine sand (blue/cyan curves) and medium sand (red/green) curves. As indicated in Figure 6, Nielsen (1992) suggested a simple 'selective entrainment' function to relate the sediment in the bed to that found in near-bed suspension. However, when interpreted as a Transfer function Tr, Nielsen's (1992) Eq. (B.1) turns out to overestimate the importance of the coarser fractions in the reference concentration (see Appendix B). It may be expected from the comparisons in Figure 6 that the same bias is inherent in fractional approaches such as that used by Wallbridge and Voulgaris (1997), motivating the use of the alternative Transfer function approach.

Figure 9 shows the same results for Tr but with the grain size normalised by the critical diameter d_c. All tests show evidence of sediment in suspension for $d/d_c > 1$ suggesting that a convective mechanism, as well as turbulent diffusion, is responsible for the upward flux of sediment. The presence in suspension of grains having $d > d_c$ is far more pronounced for the medium sand Deltaflume cases than the fine sand cases, with the steeper ripples formed in the medium sand being more capable than the low ripples in the fine sand of suspending coarser fractions. This reinforces the suggestion of a convective transfer mechanism associated with vortex shedding from the steeper ripple crests. Interestingly, the fine-sand case of MN85, in which the ripples were also steep (η/λ=0.14), exhibits a Transfer function similar to that found for some of the steeply-rippled, medium-sand cases in the Deltaflume. The scaling of grain size by d_c in isolation in Figure 9 is evidently not sufficient to explain the functional form of Tr, since the fine and medium sand groupings remain fairly distinct. So the question that arises is whether a non-dimensional scaling of

the grain diameter can be found that 'collapses' the curves in Figure 8 in a way that brings out the underlying behaviour of the Transfer function.

The scaling approach adopted in Figure 10 involves the introduction of the peak bed shear stress, together with a ripple steepness factor. The former dependence is empirically based and has been arrived at simply by noting how the ordering of the Tr curves in Figure 9 for the different tests is correlated with the values of θ' in Table 2. As far as the rippled bed effect is concerned, 'flow contraction' terms of the kind used by Nielsen (1986) have been tested, involving the general expression $(1+a_1\pi(\eta/\lambda))^{a_2}$ where $a_{1,2}$ are constants that depend upon the ripple geometry. For sinusoidal ripples the enhancement of the irrotational flow speed at the ripple crest compared with that in the free stream corresponds to $a_1=1$ and the choice $a_2=2$, which implies a quadratic friction effect, then provides an enhancement to the bed stress based on the enhancement in the near-bed flow speed. For steep natural ripple shapes Davies (1979) modelled the potential flow and showed that values of $a_1=2$ (or larger) were appropriate depending upon the detailed ripple shape. For the present tests the value $a_1=3$, combined with $a_2=2$, has been found to give the most convincing representation of the Transfer function Tr. In practice, this empirical 'flow contraction' expression (with $a_1=3$ and $a_2=2$) behaves in a closely similar manner (trend within 3%) to the ripple steepness itself for all the ripples in the present tests having $\eta/\lambda>0.05$, that is apart from f7a for which η/λ was somewhat smaller. Therefore, the rippled bed effect has been taken here simply as η/λ, with a correction made for f7a.

With both the bed stress and also rippled bed effects included, the abscissa has been scaled using the parameter X defined in Eq. (14). This draws the Tr curves together quite well and, interestingly, causes the three irregular wave tests (f7a, a9a and a10a) to stand apart from the others. This separation is highlighted in Figure 10 by the use of blue and red colours, respectively, with bold lines of each colour showing the average behaviour for that group. Figure 10a includes also the result from the experiment of MN85 which deviates from the cluster of blue curves, but nevertheless conforms to the general behaviour for regular waves. Figure 10b shows again the average Tr curves for the regular and irregular waves now accompanied by dashed curves that characterise the behaviour of Tr according to:

$$Tr = 0.5\left[1.05 - tanh\left(b_1(X - b_2)\right)\right] \quad where \quad X = \frac{d}{d_c}\frac{\theta'^{0.5}}{\eta/\lambda} \tag{14}$$

The values of the constants (b_1,b_2) corresponding to the dashed curves in Figure 10b are (0.4,4.5) for the regular waves and (0.35,7.5) for the irregular waves. The functional form in Eq. (14) has no specific physical underpinning and is included for illustration only.

It is worth noting that the quotient $\theta'^{0.5}/d_c$ that forms part of the expression for X is related to the median diameter of the bed sediment, as follows. Firstly, d_c is derived from consideration of the bed shear stress through Fredsøe and Deigaard's (1992) suspension criterion, taken here as $w_{sc} = 0.8u'_{*w}$ where w_{sc} is the settling velocity corresponding to the critical grain size d_c and u'_{*w} is the (skin) friction velocity (Eq.(12)). Secondly, since in practice most of the grain fractions in the experiments fall in Hallermeier's (1981) transitional range (134-851 μm), with only the finest fractions straying slightly into the Stokes range, the settling velocity is given by (see Eq. (C.3)):

$$\frac{w_s d}{\nu} = \frac{D_*^{2.1}}{6} \tag{15}$$

where ν is the kinematic viscosity. It follows from use of the suspension criterion and Eq. (12) that:

$$\frac{\theta'^{0.5}}{d_c} = \frac{d_c^{0.1}}{0.8\, d_{50b}^{0.5}} \left[\frac{(s-1)g}{\nu^2}\right]^{0.2} \tag{16}$$

such that the abscissa in Figure 10 is related directly to d_{50b}. This dependence might seem counterintuitive in a study focussing on the independent behaviour of individual grain fractions, but it arises from the role of d_{50b} in determining the bed shear stress, which connects with the remarks of Wiberg and Smith (1987) noted following Eq. (12).

In summary, the Transfer Function in Figure 10 shows a consistent, coherent pattern. The presence of grains in suspension with sizes greater than d_c suggests that convective effects associated with vortex shedding from the ripple crests supplement diffusion and that this is particularly important for the coarser fractions. Importantly, irregular waves seem to increase the chance that these coarser fractions are found in suspension, for both low and steep ripples (i.e. in the fine and medium sand respectively). This is very probably due to the ability of the largest waves in an irregular (here JONSWAP) sequence to entrain coarse grains episodically to significant heights above the bed by convective means. The question addressed next is whether this outcome is complemented by a behaviour in the suspension decay scale L_S that also suggests a convective upward component of the sediment flux for the coarser fractions.

6. Suspension decay scale

Here initial consideration is given to L_{ST}, the suspension decay scale (or distribution length) for the aggregated concentration profile for each test, i.e. the C-profile (Eq. (5)) corresponding to the sum of all grain fractions. This is the counterpart to the total reference concentrations shown by the open

symbols in Figure 5. It provides a baseline value and, further, it represents information that is often known from experimentally determined C-profiles.

The dimensional values of L_{ST} for the present tests, including that of MN85, are shown in Figure 11. For values of d_0/λ of about 1, momentum transfer due to vortex shedding is particularly effective. However for larger values of d_0/λ ($\geq$2), and hence larger vortex excursions horizontally, the momentum transfer process becomes progressively 'detuned' and less efficient (Malarkey and Davies, 2004; Davies and Thorne, 2008). Interestingly, for the Deltaflume cases the largest values of L_{ST} occur for d_0/λ in the range (1-1.6) corresponding to the fine sand tests, whereas somewhat lower values of L_{ST} occur for the medium sand tests with d_0/λ~2, despite the fact that the ripples were in general significantly larger in height and steepness. The results indicate also that for the irregular waves (f7a, a9a & a10a) the values of L_{ST} were relatively low for both the fine and medium sand groupings, indicating that sediment was suspended to relatively smaller heights. However, since the irregular cases do not stand distinctly apart from the regular ones, they are not treated separately in what follows. The value of L_{ST} shown for the test of MN85 is lower than the other values, as expected for a small-scale experiment. The results in Figure 11 indicate that the decay scale is not clearly related to the ripple height or steepness, as might have been expected. In contrast, the results in Figure 12 within the sub-orbital ripple range suggest that L_{ST}/λ remains roughly constant ($\approx$0.4) for both regular and irregular wave cases, with the linear behaviour ($L_{ST}/\lambda \sim d_0/d_{50b}$) indicated by the dashed line in the orbital range offering a tentative description that matches the laboratory result of MN85 quite well.

While L_{ST} provides a baseline value, the central question here involves the behaviour of the L_S values for the individual fractions. Figure 13 shows the L_S distributions for the four representative tests illustrated in Figure 6, including the irregular wave f7a and the small-scale test of MN85. Also shown for comparison are results based on four formulations for L_S, namely: i) Nielsen's (1990) formulation developed for sharp crested ripples (Eqs.(5 & 11)) in the same (RE, a_1/k_s) turbulent flow parameter ranges as indicated in Appendix B; ii) a 'pure diffusion' formulation for $L_S = \varepsilon_s/w_s$ with ε_s based on Eqs.(2 & 3) involving Nielsen's (1992) expression for very rough beds and with w_s based on Hallermeier's (1980) formulation (see Appendix C); iii) an equivalent formulation for $L_S = \varepsilon_s/w_s$ based on Van Rijn's (1989) expression for ε_s (Eq.(9)), derived for RE=(0.1-0.3)$\times 10^5$ and A_1/k_s~0.4, combined again with Hallermeier's settling velocity; and iv) an updated formulation based on Van Rijn's (2007a) more recent expression for ε_s. As noted in §2 formulation iv) has the same nature as Eq. (9), but with the value of β capped at 1.5. Each of these formulations, here applied on the assumption

that the individual fractions do not interact with each other, predicts a decreasing decay scale as fraction size increases, but with a magnitude generally smaller than observed. The two formulations arising from Nielsen's expressions ((i) and (ii)) have the same behaviour but slightly different magnitudes for the larger fractions, but they differ for the smaller fractions with Nielsen's (1990) Eq.(11) predicting that L_S here remains constant. There is no sign of such an effect in the data either from the Deltaflume or from the experiment of MN85. In contrast, due to its inclusion of D_* on the right hand side of Eq.(9), the formulation for L_S arising from Van Rijn's (1989) expression has the behaviour $D_*/w_s \sim d^{-1}$ in the Stokes settling regime and $D_*/w_s \sim d^{-0.1}$ in the transitional regime (see Appendix C), which explains the change in slope seen in the respective curves in Figure 13. The resulting, almost invariant, predicted behaviour for L_S for the larger fractions agrees quite well with the experimental evidence, particularly for the case of MN85. In effect, implicit in Van Rijn's (1989) formulation is a strong convective effect where the larger grain fractions are concerned, almost identical to Fredsøe and Deigaard's (1992) 'pure convection' model discussed in §2.3. In contrast, the more recent formulation of Van Rijn (2007a) is more akin to a diffusive approach, as is particularly evident for the two medium sand cases. However, had the value of β not been capped at 1.5, this formulation would actually have behaved more along the lines of Van Rijn (1989), showing a 'flattening out' of L_S for the larger fractions. For the two fine sand tests, it produces better agreement with the present data than the other formulations, and particularly so for irregular wave case f7a. Van Rijn's (2007a) formulation was designed for prototype and field scales; when applied to the small-scale laboratory case of MN85 in Figure 13, it produces rather exaggerated L_S values.

In order to assess the convective contribution that can be inferred from the present data, the results for L_S are compared in Figure 14 with a scaled version of Nielsen's (1992) 'pure diffusion' expression (ii) above, which has been forced to match the observed value of L_S for the smallest fraction in each test. The change in slope of the 'pure diffusion' curves is due to the change from the Stokes to the transitional settling regime. To a greater or lesser extent the observed distributions depart from the 'pure diffusion' behaviour, tending to exhibit a less rapid decrease in L_S for the largest fractions. This suggests a convective contribution to the upward flux for these larger fractions and it supports the inference of such an effect in the reference concentrations and Transfer function in §5. The convective effect is particularly pronounced in fine sand tests f5a and f8a, and also in the experiment of MN85. Where it is less pronounced is in tests f7a and a9a, both involving irregular waves; the third test with irregular waves (a10a) would also fit into this pattern had the curve matching been carried out using the second, not the smallest fraction in suspension. Despite this, the irregular wave cases are not treated separately in what follows.

In order to systematise the decay scales, L_S has been non-dimensionalised by L_{ST} and then plotted for each test using parameter X again on the abscissa, c.f. Figure 10. Figure 15a shows that with the results plotted logarithmically the curves are reasonably well clustered together with a change of slope in L_S / L_{ST} at about X=7. The low-wave test f3a appears as an outlier on the 'low' side of the general trend, while the test of MN85 appears on the 'high' side. The results for L_S/L_{ST} from each Deltaflume test have been interpolated linearly with increment 0.1 in X, and have then been averaged together to yield the black bold line shown. The jagged appearance of this line at both ends is due to the decreasing number of tests available for averaging for both small and large grain sizes.

The average curve for L_S/L_{ST} is repeated in Figure 15b together with a simple representative two-part, power law, curve fit:

$$\frac{L_S}{L_{ST}} = c_3 X^{c_4} \tag{17}$$

with the coefficients (c_3,c_4) equal to (3.63,−1.1) for X<7 and (0.82,−0.3) for X>7. Noting as before that the bulk of the grain fractions fall into Hallermeier's transitional settling range (c.f. Eq.(15)), the line slope (−1.1) for the smaller grain fractions corresponds to a diffusive behaviour similar to the 'pure diffusion' curves in Figure 14. In contrast, the line slope (−0.3) for the larger fractions suggests an additional, convective, component in the upward sediment flux. Had the line slope become zero for X>7, there would have been a suggestion of 'pure convection' as in the model of Fredsøe and Deigaard (1992) and the similar model of Van Rijn (1989). As it turns out the present Deltaflume data lies between these two extremes, with the slope −0.3 suggesting a combined convective + diffusive sediment flux for X>7. The convective behaviour appears to be more pronounced in the case of the laboratory experiment of MN85 than in the Deltaflume tests.

7. Application of the Transfer function and decay scale L_S to determine the suspended sediment grain size profile (d_{50s})

In order to assess the empirical relations derived in §5 and §6, these have been used to calculate the vertical profile of d_{50s} in each Deltaflume test (Figure 16) for comparison with the profile determined from the sieve analysis carried out at each sampling height. For the representative height of 0.1m above the ripple crest, the observed ratio d_{50s}/d_{50b} was in the range 0.49-0.68 with the bed sediment having d_{90}/d_{10}=3.2-4.3, consistent with the findings of Van Rijn (2007b) (see §2.1). The predicted profiles of d_{50s} in Figure 16 were based on i) the cumulative size distribution for the

bed sediment, ii) the Transfer function (Eq. (13)) defined according to the distinction made (Eq.(14)) between regular and irregular waves and iii) the decay length scale relationship given by Eq. (17) with L_{ST} corresponding to the dashed line representation in Figure 12. The steps involved in the calculation are included in Appendix D. No further 'adjustment' or 'fitting parameter' was used in the individual cases to match the calculated values of d_{50s} to the measured distributions. The case of MN85 is not included since these authors did not present a size profile for comparison.

The profiles in Figure 16 provide a generally convincing match with the measurements of d_{50s}, demonstrating the applicability and self-consistency of the empirical approaches. The overall difference between the median diameter of the bed sediment and that in suspension is well predicted, and the rate of decrease in d_{50s} with increasing height is also generally well predicted. Test f3a involving the lowest wave height and smallest ripple wavelength is less well predicted than the others due primarily to the poor agreement between the observed and predicted values of L_{ST} in this case. Clearly, due to the circular nature of the argument, the results for d_{50s} in Figure 16 cannot be considered as an independent check on the empirical relations proposed in §5 and §6. Nevertheless, they suggest that the simple procedure might be sufficiently robust to be worth testing against independently derived field or (large-scale) laboratory data.

The subplot in Figure 16 for test a8a includes the d_{50s} profile presented for this case by Davies and Thorne (2002). This was obtained from an intra-wave numerical modelling exercise in which the sediment in suspension was assumed to have size $d < d_c$, which corresponded to about 15% of the bed material by volume. This sediment was subdivided into 5 volumetrically equal fractions and the d_{50s} profile was obtained by a procedure similar to that used above. The results for d_{50s} are less satisfactory than those derived using the present approaches. Evidently this earlier work failed to represent the coarser nature of the near-bed suspended sediment by its neglect of those grains having $d > d_c$. Its rather better description of d_{50s} at the uppermost measurement levels occurs due to the differences in modelling approaches.

8. Discussion

8.1 Prototype versus laboratory experimental conditions

The results in Figure 15 show that for the MN85 laboratory experiment there was considerably less variation in L_S/ L_{ST} with relative grain size than found in the Deltaflume tests. As noted in §6 the MN85 results exhibit a pronounced convective behaviour with the value of L_S varying by only a factor

of just less than 2 from the finest to coarsest fractions. In order to explain this rather different behaviour between the full-scale prototype and small-scale laboratory experiments, the possibility of a wave period effect on the measured C-profiles has been considered, following the approach taken by Dohmen-Janssen et al. (2002) to represent 'phase-lag' effects. However this has not been found to explain the small amount of variation in L_S/ L_{ST} found for MN85, which probably relates to the results in Figures 3 (and 12) where it was shown that this test was carried out in the orbital regime while the Deltaflume tests were in the sub-orbital regime, with the associated implications for the effectiveness of vortex shedding discussed in §4.2 and §6. For the steep ripples in test of MN85, $L_{ST} /\eta \approx 1$ suggesting a convective layer thickness that scales on the ripple height, with the sediment being largely confined to this layer. In contrast, the values of L_{ST} /η for the Deltaflume were 2 to 4 for the medium sand and 5 to 15 for the fine sand, indicating a far thicker, more diffuse mixing layer. The pronounced convective effects in the orbital regime for MN85 would seem to have given rise to the fairly constant values of L_S observed for the 4 coarsest fractions, whereas the greater variation in L_S in the Deltaflume tests indicates a more gradual transition from diffusion to convection as the fraction size increases. This suggests a distinction between the organised and repeatable pattern of eddy shedding that occurs in the orbital regime, which promotes convection, and the less efficient, 'detuned' process in the sub-orbital regime that results in diffusion playing a significant complementary role. The 'detuning' effect above steep ripples is associated with larger values of d_0/λ (see §4.2). It seems that Nielsen's (1992) interpretations of convective processes were guided by observations made in the orbital regime and, where field or prototype observations are concerned, the pure-convective signature that he identified becomes less pronounced.

8.2 'Concave' versus 'convex' mean C-profiles

Based on the MN85 data for non-breaking waves over rippled beds and also field data, Nielsen (1992) suggested that the shape of mean C-profiles varies from upward convex for finer fractions to upward concave for coarser fractions. For the MN85 data he suggested convex (diffusive) C-profile shapes for fractions having $d < 0.1$mm in the height range $z \leq 0.07$ m and concave (convective) shapes for $d > 0.3$ mm for all heights z. Tomkins et al. (2003) made similar observations above a rippled bed of mixed quartz and heavy mineral sand. Above 0.02 m they found that all grain classes displayed a similar vertical length scale L_S despite their different settling velocities. Nearer to the bed the relative concentration profiles displayed a transition from upward concave to upward convex as the sediment size became finer. In contrast, Sistermans (2002) observed no such behaviour in oscillatory flow above ripples, despite measuring C-profiles with good near-bed resolution. Although in the present Deltaflume data there is evidence of convex profile shapes in the near-bed layer in

certain tests (e.g. f8a), a consistent pattern has not been found in the data set as a whole, due possibly to there being rather few pumped sample heights in $z < 0.1$m.

As noted in §2.2 Nielsen and Teakle (2004) proposed a 'finite mixing length' [FML] approach that accounts for higher derivatives in vertical C-profiles than are involved in the classical Fickian diffusion theory. They suggested that FML effects become more important for coarser fractions in suspension, since such grains exhibit smaller L_S values and therefore require a description that accounts for the third derivative of concentration $\partial^3 C/\partial z^3$. This allows convex C-profiles to be explained in the very near-bed layer O(0.05 m) for fine fractions, compared with the concave profiles seen for coarser grains in the same flow. The convex C-profile behaviour is explained by Teakle and Nielsen (2004) in terms of the height at which the Fickian sediment diffusivity achieves a maximum value. This maximum occurs, in practice, *only* for finer sediment fractions, with the resulting convex behaviour being observed, for example, in MN85 in $z < 0.07$m. In the Deltaflume tests, the maximum in the Fickian diffusivity based on Teakle and Nielsen's (2004) argument occurs at 0.081, 0.135 and 0.136 m above the bed for tests f5a, f8a and a8a, respectively. The convex profile effect might have been observed therefore for the finer grains fractions with better vertical resolution near the bed. The analysis of the Deltaflume data in §6 has simply involved a height-constant diffusivity ε_s. Neither this profile nor a 'constant + linear' Fickian profile (see Appendix A) exhibits a near-bed maximum of the kind implicit in the FML approach.

9. Conclusions

The relationship between the grain size distribution of the sediment on the bed and that found in suspension due to wave action above ripples has been assessed using detailed, pumped sample, measurements obtained at full-scale in the Deltaflume (of Deltares, The Netherlands) and also at laboratory scale in an experiment carried out by MN85. The measured suspended concentrations have been split into multiple fractions and interpreted using exponential C-profile curve fitting. The Transfer Function defined to relate the bed sediment size distribution to that of the reference concentration shows a consistent, coherent pattern. While indicating that finer fractions are relatively easily entrained, it indicates also that grains are found in suspension with sizes greater than the critical size d_c based on the suspension criterion of Fredsøe and Deigaard (1992). This suggests that the suspension is caused in part by convective effects that supplement diffusion, which becomes particularly important for the coarser fractions. The evidence for convective effects, via the Transfer Function Tr, is more pronounced for the medium sand bed than the fine sand bed in the

Deltaflume, due mainly to the large and small ripple steepness in the respective cases. Essentially, lower ripples tend to give rise to the dominance of diffusion while steeper ripples to convection associated with vortex shedding from the ripple crests, particularly where the coarser suspended fractions are concerned. The 'natural bed' test carried out by MN85, which involved large ripple steepness (η/λ=0.14), fits into this pattern.

The Transfer function suggests further that irregular waves increase the occurrence of coarser fractions in suspension. This is probably due to the ability of the largest waves in a sequence to entrain sediment episodically to significant heights above the bed by convective means. The irregular wave effect is included in the function determined to best represent Tr. The proposed, tentative, curve fit (Eq. (14)) expresses Tr as a function of a parameter X that non-dimensionalises the grain fraction diameter d by the critical diameter d_c, the ripple steepness η/λ and the peak Shields parameter θ'.

The exponential decay scales L_S arising from the C-profiles for the individual fractions have been examined in order to assess the mechanisms responsible for the upward transfer of sediment grains. The aggregated decay scale L_{ST} has been found to depend upon the ripple wavelength with $L_{ST} \approx 0.4\lambda$ for the prototype Deltaflume cases. The variation of L_S in each test around this reference value L_{ST} has been compared with established formulations from which it has been concluded that, for finer fractions in suspension having X<7, the C-profiles are characteristic of a purely diffusive process. In contrast, for fractions having X>7 a combined convective + diffusive upward transfer of grains is suggested. The behaviour of L_S/ L_{ST} (Eq. (17)) follows the power law behaviour $\sim X^m$ with m= -1.1 and -0.3 in the respective ranges of X. Pure convection corresponds to m = 0 in which case all C-profiles become the same regardless of the grain size. The slope -0.3 found for the Deltaflume cases suggests a convective contribution to the upward flux of grains therefore. The laboratory test of MN85 fits into this scheme, though with a suggestion of a more pronounced convective behaviour than found in the Deltaflume. There is evidence also that wave irregularity inhibits suspension through lowering the value of L_S somewhat, though this effect is less pronounced than the corresponding effect seen in the Transfer function. This suggests that, while the largest waves in an irregular sequence cause the suspension of coarser grains from the bed, the process sustaining the suspension becomes less effective when the repetitive nature of the eddy shedding mechanism is compromised by irregularity.

The separate findings for the Transfer function Tr and the exponential decay scale L_S present supporting evidence of diffusion affecting the finer grain fractions in suspension and combined diffusion + convection affecting the coarser fractions. The present study has focussed on natural mixtures of grains that do not present a large dynamic range via, say, the geometric standard deviation. So while the parameterisations derived for Tr and L_S should be applicable to sediment with a fairly broad size distribution, they are not necessarily going to work as well outside the experimental ranges considered here.

Acknowledgements

This work was supported by the Natural Environment Research Council (NERC, UK) 'COHBED' grant (NE/1027223/1), EU HYDRALABIV JRA WISE, NOC national capability funds and also the EU through its Access to Large Scale Facilities under contract MAS3-CT97-0106. The authors would particularly like to thank Dr Jon J Williams who co-ordinated the experiment and Mr John D. Humphery, Mr Peter J. Hardcastle and Dr Paul S Bell who were central to the deployment of the instrumentation. We would also like to thank Mr John O. Malcolm whose company Sediment Analysis Services carried out the particle size sorting analysis. Finally, the reviewers are thanked for some perceptive comments.

References

Bosman J. J., van der Velden E. and C.H. Hulsbergen, 1987. Sediment concentration measurements by transverse suction, Coastal Engineering, 12, 353–371.

Coleman N.L., 1981. Velocity profiles with suspended sediment. Journal of Hydraulic Research, 19, 3, 211-229.

Davies A.G., 1979. The potential flow over ripples on the seabed. Journal of Marine Research, 37, 4, 743-759.

Davies A.G. and P.D. Thorne, 2002. 1DV-model of sand transport by waves and currents in the rippled bed regime. Proceedings of 28th International Conference on Coastal Engineering, Cardiff, World Scientific, 2599-2611.

Davies A.G. and Thorne P.D., 2005. Modelling and measurement of sediment transport by waves in the vortex ripple regime. Journal of Geophysical Research, 110, C05017, doi:10.1029/2004JC002468

Davies A.G. and Thorne P.D., 2008. Advances in the Study of Moving Sediments and Evolving Seabeds. Surveys in Geophysics, 29,1-36. DOI 10.1007/s10712-008-9039-x. Available at: http://dx.doi.org/10.1007/s10712-008-9039-x

Davies A.G. and C. Villaret, 1997. Oscillatory flow over rippled beds: Boundary layer structure and wave-induced Eulerian drift. Chapter 6 in Gravity Waves in Water of Finite Depth, ed. J.N. Hunt, Advances in Fluid Mechanics, Computational Mechanics Publications, 215-254.

Day T.J., 1980. A study of the transport of graded sediments. Hydraulics Research Wallingford U.K., Report IT 190, 10pp.

Dohmen-Janssen C.M., Kroekenstoel D.F., Hassan W.N. and J.S. Ribberink, 2002. Phase lags in oscillatory sheet flow: experiments and bed load modelling. Coastal Engineering, 46, 1, 61-87.

Egiazaroff I.V., 1965. Calculation of nonuniform sediment concentrations. Journal of the Hydraulics Division, Proceedings of the American Society of Civil Engineers, 93, HY4, 281-287.

Hallermeier R.J., 1981. Terminal settling velocity of commonly occurring sand grains. Sedimentology, 28, 6, 859-865.

Fredsøe J. and R. Deigaard, 1992. Mechanics of Coastal Sediment Transport. Advanced Series on Ocean Engineering, Volume 3. World Scientific, Singapore, 369 pp.

Hassan W.N.M., 2003. Transport of size-graded and uniform sediments under oscillatory sheet-flow conditions. PhD Dissertation, University of Twente, The Netherlands, ISBN 90-365-1899-x

Li Z. and A.G. Davies, 2001. Turbulence closure modelling of sediment transport beneath large waves. Continental Shelf Research, 21, 3, 243-262.

Malarkey, J., and A. G. Davies, 2004. An eddy viscosity formulation for oscillatory flow over vortex ripples. Journal of Geophysical Research, 109, C12016, doi:10.1029/2003JC002086

Malarkey J., Magar V. and Davies A.G., 2015. Mixing efficiency of sediment and momentum above rippled beds under oscillatory flows. Continental Shelf Research, 108, 76-88. http://dx.doi.org/10.1016/j.csr.2015.08.004

Masselink G., Austin M.J., O'Hare T.J. and P.E. Russell, 2007. Geometry and dynamics of wave ripples in the nearshore zone of a coarse sandy beach. Journal of Geophysical Research, 112, C10022, doi:10.1029/2006JC003839

McFetridge W.F. and P. Nielsen, 1985. Sediment suspension by non-breaking waves over rippled beds. Technical Report UFL/COEL-85/005, Coastal and Oceanographical Engineering Department, University of Florida, Gainesville, 131pp.

Nelson T.R., Voulgaris G. and P. Traykovski, 2013. Predicting wave-induced ripple equilibrium geometry. Journal of Geophysical Research: Oceans, 118, 3202-3220.

Nielsen, P., 1983. Entrainment and distribution of different sand sizes under water waves. Journal of Sedimentary Petrology, 53, 2, 423-428.

Nielsen P., 1986. Suspended sediment concentrations under waves. Coastal Engineering, 10, 23-31.

Nielsen P., 1990. Coastal bottom boundary layers and sediment transport. In P. Bruun ed. Port Engineering (4th edition), Volume 2, 550-585.

Nielsen P, 1992. Coastal Bottom Boundary Layers and Sediment Transport. Advanced series on ocean engineering, volume 4. World Scientific, Singapore, 324 pp.

Nielsen P. and I.A.L. Teakle, 2004. Turbulent diffusion of momentum and suspended particles: a finite-mixing-length theory. Physics of Fluids, 16, 7, 2342-2348.

O'Donoghue T. and S. Wright, 2004. Flow tunnel measurements of velocities and sand flux in oscillatory sheet flow for well-sorted and graded sands. Coastal Engineering, 51, 1163-1184.

Sengupta S., 1979. Grain-size distribution of suspended load in relation to bed materials and flow velocity. Sedimentology, 26, 63-82.

Sistermans P.G.J, 2002. Graded sediment transport by non-breaking waves and a current. Communications on Hydraulic and Geotechnical Engineering, Faculty of Civil Engineering and Geosciences, Delft University of Technology, Report No. 02-2, ISSN 0169-6548 (and also PhD Dissertation, Delft University of Technology, ISBN 90-9016368-9).

Sleath J.F.A., 1991. Velocities and shear stresses in wave-current flows. Journal of Geophysical Research, 96, C8, 15,237-15,244.

Soulsby R.L., Whitehouse R.J.S. and K. Marten, 2012. Prediction of time-evolving sand ripples in shelf seas. Continental Shelf Research, 38, 47-62.

Swart D.H., 1976. Predictive equations regarding coastal transports. Proceedings of 15th International Conference on Coastal Engineering, Honolulu, Hawaii, Chapter 66, 1113-1132.

Teakle I.A.L. and P. Nielsen, 2004. Modelling suspended sediment profiles under waves: a Finite-Mixing-Length theory. Proceedings of 29th International Conference on Coastal Engineering, 1780-1792.

Thorne P.D., Williams J.J. and A.G. Davies, 2002. Suspended sediments under waves measured in a large-scale flume facility. Journal of Geophysical Research (Oceans), 107 (C8), 10.1029/2001JC000988, 16pp.

Thorne P.D., Davies A.G. and Bell P.S., 2009. Observations and analysis of sediment diffusivity profiles over sandy rippled beds under waves, Journal of Geophysical Research, 114, C02023, doi:10.1029/2008JC004944

Tomkins M.R., Nielsen P. and M.J. Hughes, 2003. Selective entrainment of sediment graded by size and density under waves. Journal of Sedimentary Research, 73, 6, 906-911.

Van Rijn L.C., 1984. Sediment transport, Part II: Suspended load transport. Journal of Hydraulic Engineering, 110, 11, 1613-1641.

Van Rijn L.C., 1989. Handbook of sediment transport by currents and waves. Delft Hydraulics, The Netherlands, Report H 461.

Van Rijn L.C., 1993. Principles of Sediment Transport in Rivers, Estuaries and Coastal Seas. Aqua Publications –I11, Amsterdam, the Netherlands. ISBN 90-800356-2-9.

Van Rijn L.C., 2007a. Unified view of sediment transport by currents and waves. 2: Suspended transport. Journal of Hydraulic Engineering, 133(6):668-689.

Van Rijn L.C., 2007b. Unified view of sediment transport by currents and waves. 3: Graded beds. Journal of Hydraulic Engineering, 133(7):761-775.

Wallbridge S. and G. Voulgaris, 2007. Fractional threshold of motion for mixed sand beds and implications for sediment transport modelling. Proceedings of Coastal Dynamics '97, Plymouth, ed. E.B. Thornton, American Society of Civil Engineers, 68-77.

Wallbridge S., Voulgaris G., Tomlinson B.N. and M.B. Collins, 1999. Initial motion and pivoting characteristics of sand particles in uniform and heterogeneous beds: experiments and modelling. Sedimentology, 46, 17-32.

Wiberg P.L. and J.D. Smith, 1987. Calculations of the critical shear stress for motion of uniform and heterogeneous sediments. Water Resources Research, 23, 8, 1471-1480.

Wiberg P.L. and C.K. Harris, 1994. Ripple geometry in wave-dominated environments. Journal of Geophysical Research, 99, C1, 775-789.

Williams J.J., Bell P.S., Coates L.E., Hardcastle P.J., Humphery J.D., Moores S.P., Thorne P.D and K Trouw, 1998. Evaluation of field equipment used in studies of sediment dynamics. Proudman Oceanographic Laboratory Report No. 53, 45pp.

Tables

Test	Waves	H, H_s (m)	T, T_p (s)	Sand	η(m)	λ(m)	η/λ
f3a	regular	0.435	5	fine	0.018	0.21	0.0857
f5a	regular	0.815	5	fine	0.034	0.52	0.0654
f7a	irregular	0.784	4.743	fine	0.017	0.40	0.0425
f8a	regular	1.066	5	fine	0.063	0.84	0.0750
a8a	regular	0.811	5	medium	0.047	0.35	0.1343
a9a	irregular	0.788	4.92	medium	0.045	0.32	0.1406
a10a	irregular	1.066	5.1	medium	0.046	0.39	0.1179
a11a	regular	1.299	5	medium	0.065	0.51	0.1275
a20a	regular	1.027	4	medium	0.040	0.29	0.1379
a21a	regular	0.617	6	medium	0.040	0.28	0.143
MN85	regular	0.13	1.51	fine	0.011	0.078	0.140

Table 1. Deltaflume parameter settings together with those for the test of MN85: wave height (H,H_s), and period (T,T_p), ripple height (η), wavelength (λ) and steepness (η/λ)

Test	U_1 (m/s)	A_1 (m)	d_0 (m)	U_2 (m/s)	f_w	d_c (μm)	θ′	RE×10^{-5}	A_1/k_s	Grain fractions
f3a	0.2183	0.1737	0.3474	0.0048	0.0128	124.7	0.1165	0.29	4.5	9
f5a	0.4089	0.3254	0.6508	0.0169	0.0107	191.3	0.3400	1.02	5.9	10
f7a	0.3792	0.2862	0.5725	0.0123	0.0111	181.6	0.3031	0.83	15.8	10
f8a	0.5349	0.4256	0.8513	0.0289	0.0099	236.3	0.5409	1.74	3.6	12
a8a	0.4069	0.3238	0.6476	0.0167	0.0132	209.7	0.2049	1.01	2.1	14
a9a	0.3912	0.3063	0.6126	0.0147	0.0134	203.9	0.1927	0.92	1.9	12
a10a	0.5416	0.4396	0.8792	0.0315	0.0120	260.5	0.3303	1.82	3.2	12
a11a	0.6518	0.5187	1.0373	0.0430	0.0114	301.5	0.4555	2.58	2.5	15
a20a	0.4227	0.2691	0.5381	0.0084	0.0140	223.0	0.2347	0.87	2.0	11
a21a	0.3404	0.3250	0.6500	0.0196	0.0132	178.2	0.1432	0.85	2.3	12
MN85	0.247	0.0594	0.1187	0.031	0.0190	156.6	0.2082	0.11	1.5	6

Table 2. Derived parameters: near-bed velocity amplitude (first harmonic U_1, second harmonic U_2) based on reduced wave heights for the Deltaflume tests, orbital excursion amplitude (A_1), orbital diameter (d_0), critical grain diameter in suspension (d_c), peak Shields parameter (skin friction) θ', wave Reynolds number RE ($=U_1A_1/\nu$), relative roughness (A_1/k_s) (with k_s given by Eq. (4)), and the number of analysed grain fractions available for each test.

Figures

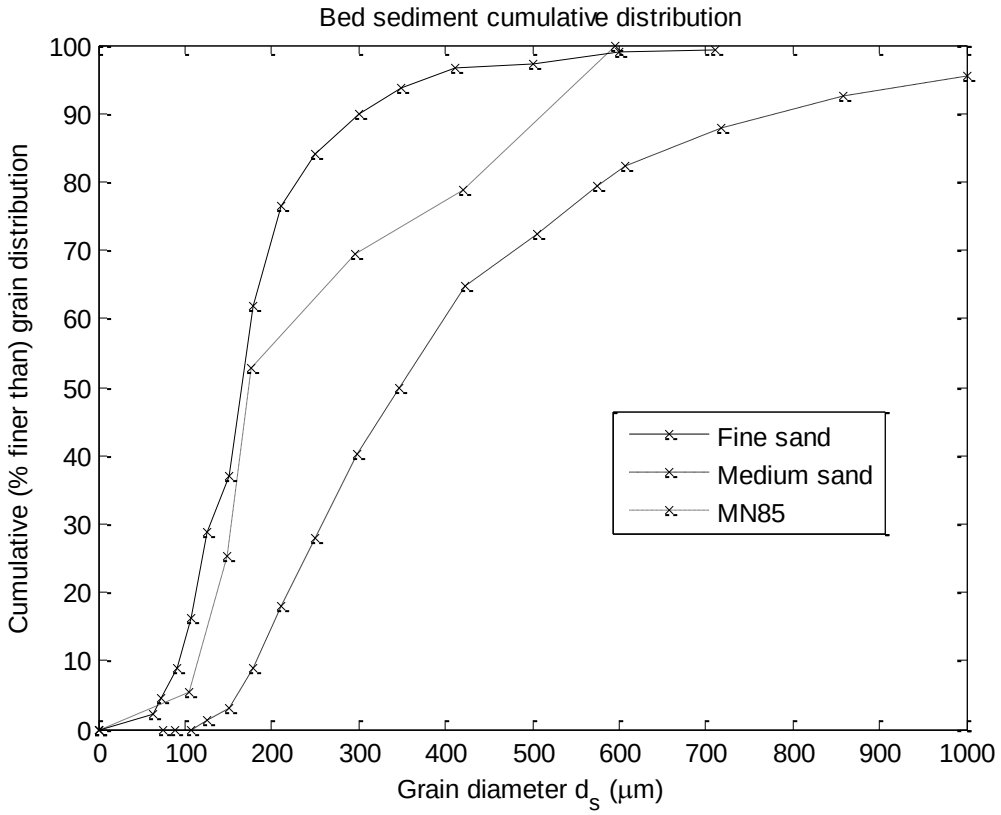

Figure 1. Bed sediment cumulative (%-finer) distribution curves determined by standard sieving for the fine and medium sand sizes in the Deltaflume and also for the fine sand used in the laboratory experiment of MN85. The crosses (x) correspond on the abscissa to the grain diameters given by the sieve sizes used in the analysis.

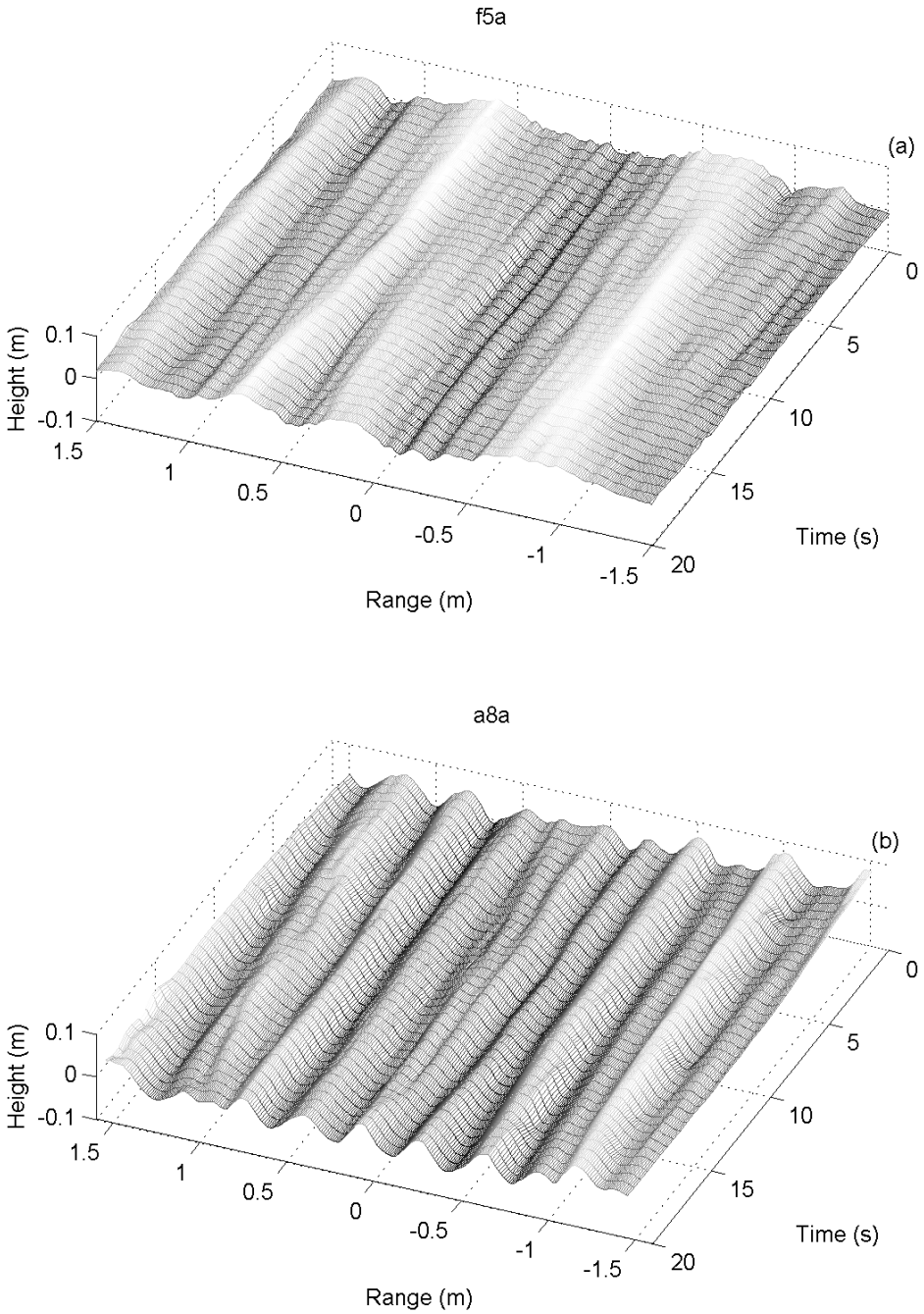

Figure 2. Ripple profiles measured successively over a 3 m bed transect with the Acoustic Ripple Profiler (ARP) during tests a) f5a (fine sand) and b) a8a (medium sand). Experimental recording time (1024 s or about 17 min) is shown on the second horizontal axis and bed height (m) on the vertical axis. The ripple steepness in a8a was approximately double that in f5a.

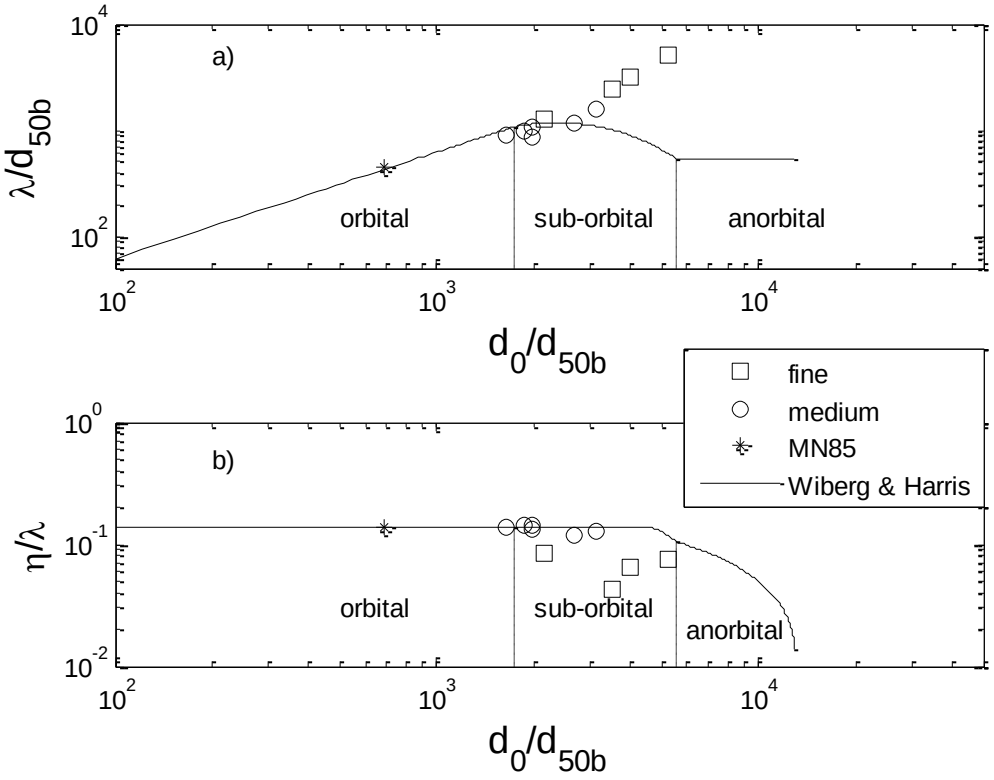

Figure 3. Normalised ripple dimensions: measured (symbols) and predicted (lines) using a modified version of Wiberg and Harris' (1994) formulation. Figure a): wavelength (λ) versus orbital diameter ($d_0=2A_1$), normalised in each case byd_{50b}. Figure b): ripple steepness (η/λ) versus normalised orbital diameter. The symbols refer to the fine and medium sand tests from the Deltaflume and also the laboratory test of MN85.

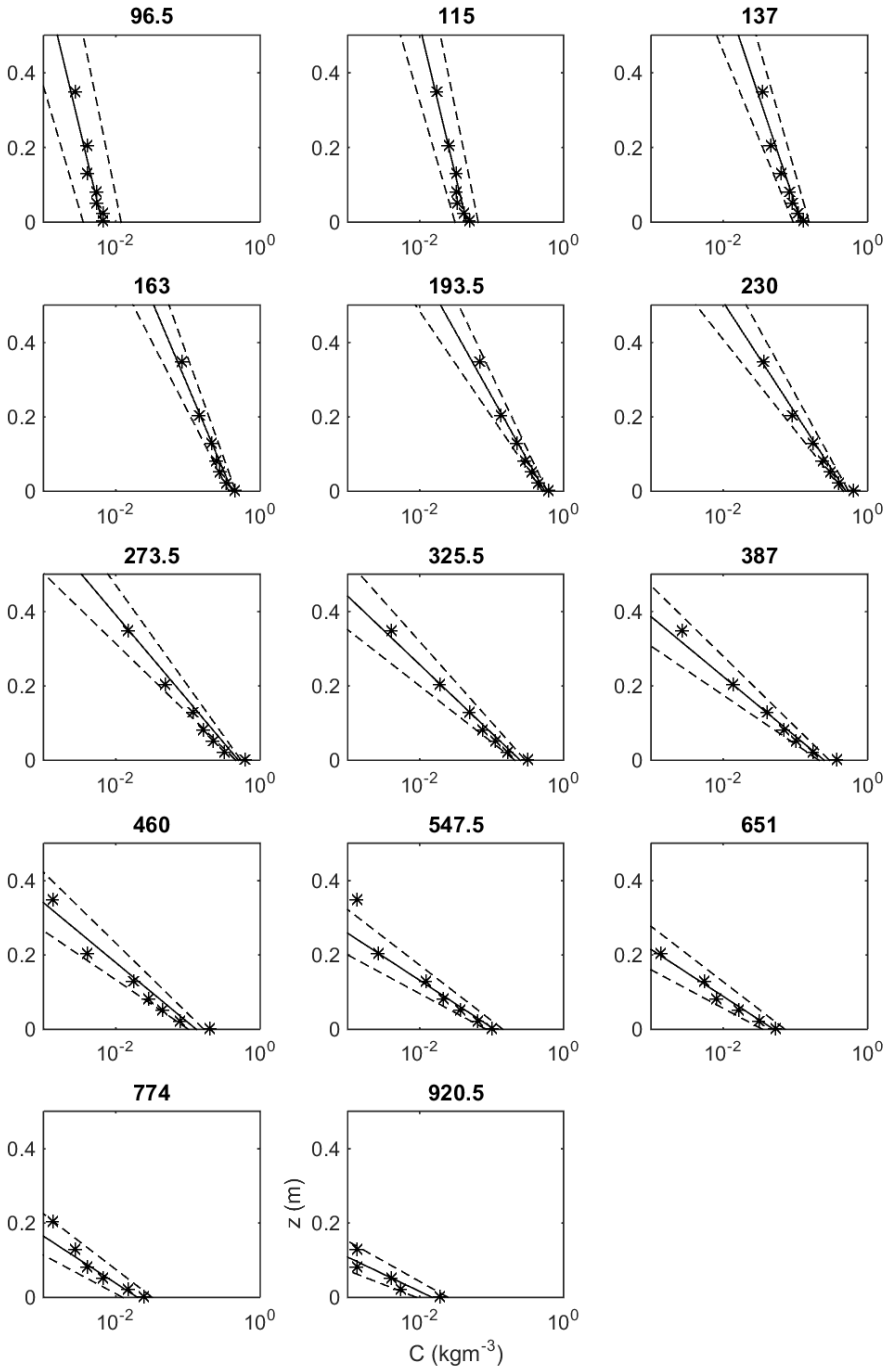

Figure 4. Example of the mean concentration profiles obtained by pumped sampling (∗ symbols) for the 14 grain fractions analysed for test a8a (medium sand). The sieve mid-interval size d_m shown above each figure indicates the nominal grain fraction size in μm. Height above the crest level (m) is shown on the linear vertical axis and concentration (kg/m^3) is plotted logarithmically on the horizontal axis. The best exponential fit to the 14 C-profiles is shown as the straight line in each subplot, together with 95% confidence limits for each fraction (dashed lines).

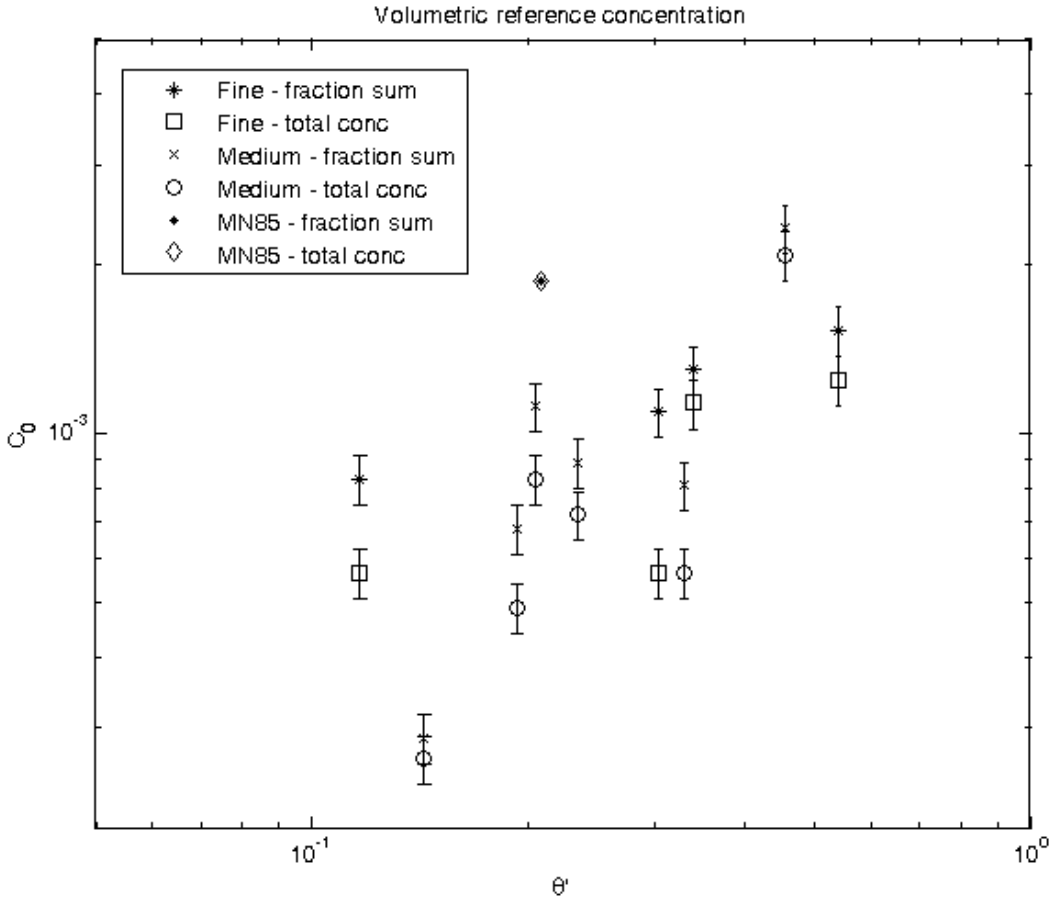

Figure 5. Volumetric reference concentrations obtained by fitting log-linear (i.e. exponential) C-profiles to the measured concentrations, together with standard deviation error bars arising from the regression analysis for C_0. For each test two reference concentration values are plotted against the corresponding peak Shields parameter (skin friction): the symbols ∗, x and • show the result of summing the reference concentrations for individual grain fractions in a test, while the symbols □, O and ◊ show the result obtained for a single curve fit to the aggregated C-profile.

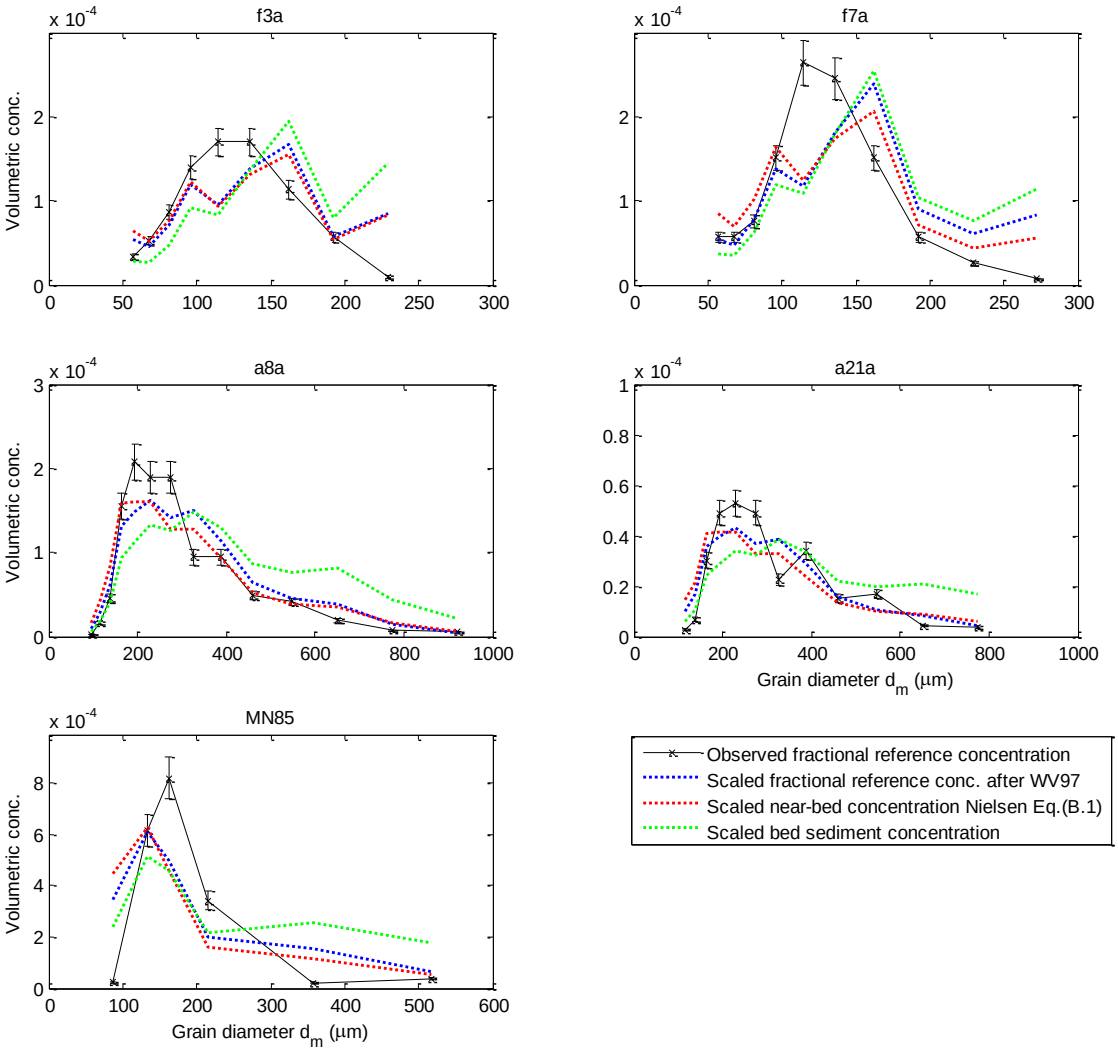

Figure 6. Volumetric reference concentrations (crosses), with standard deviation error bars, determined from exponential curve fitting for each grain fraction (c.f. Eq.(5)) in two tests with fine sand (f3a and f7a) and two with medium sand (a8a and a21a). f7a is corresponds to an irregular wave. Also shown is the distribution determined by MN85. Grain diameter denotes the central diameter d_m for each sieve interval determined at the respective mid-points on the ϕ scale, c.f. Figure 4. The dashed lines show a calculated fractional reference concentration (blue) following Wallbridge and Voulgaris (1997) [WV97], and a near-bed concentration (red) based on Nielsen's (1992) approach, in comparison with the bed sediment distribution (green). Each dashed line uses the same values of d_m as the observations, and each is scaled to have the same aggregated sum as the observed reference concentration.

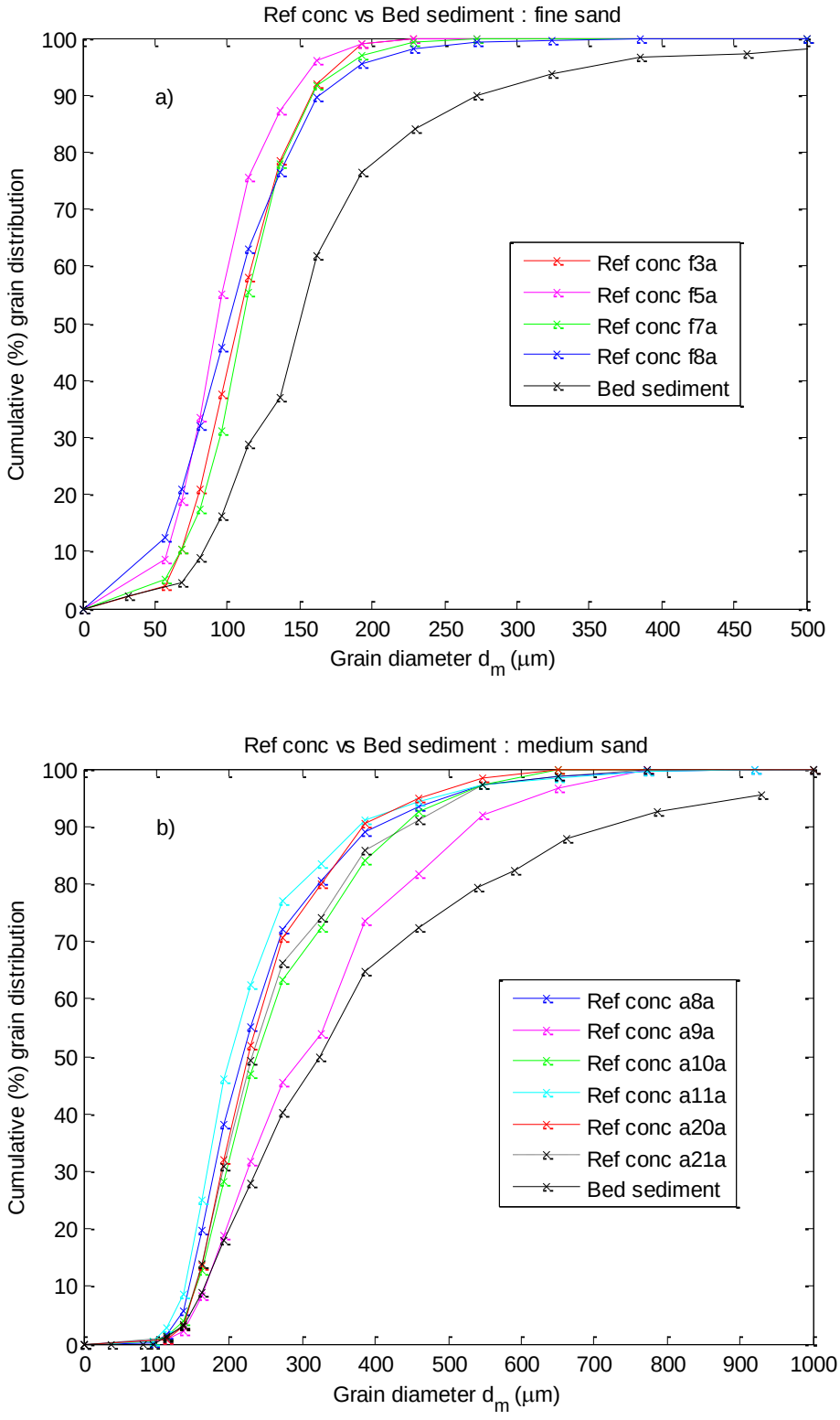

Figure 7. Cumulative size distributions for the reference concentrations in the respective Deltaflume tests compared with the distribution for the corresponding bed material. Figure a) shows results for the fine sand, and b) for the medium sand. The distribution for the bed sediment is plotted at the central diameter d_m for each sieve interval determined at the respective mid-points on the ϕ scale; therefore these bed distributions differ from the %-finer distributions shown in Figure 1.

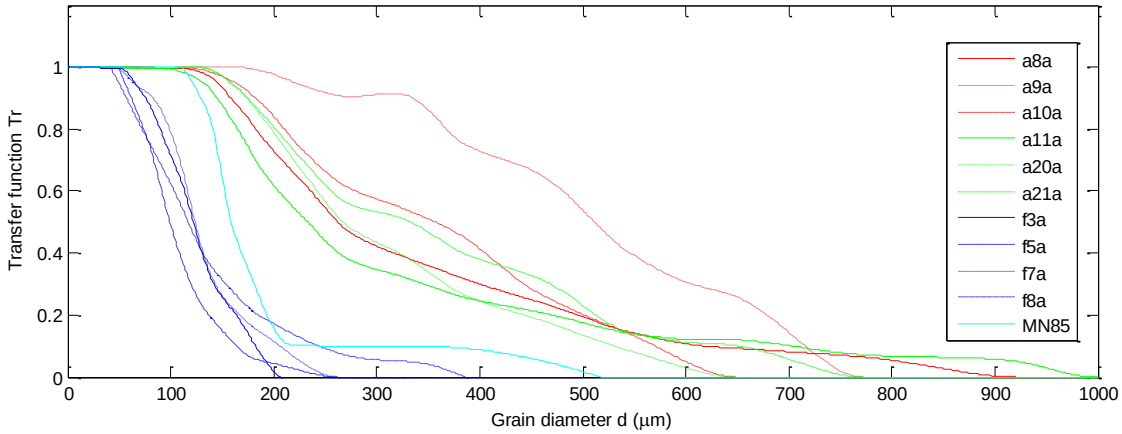

Figure 8. Transfer function Tr plotted against interpolated sediment grain size d for all Deltaflume tests with the fine and medium sand beds, and also for the laboratory test of MN85.

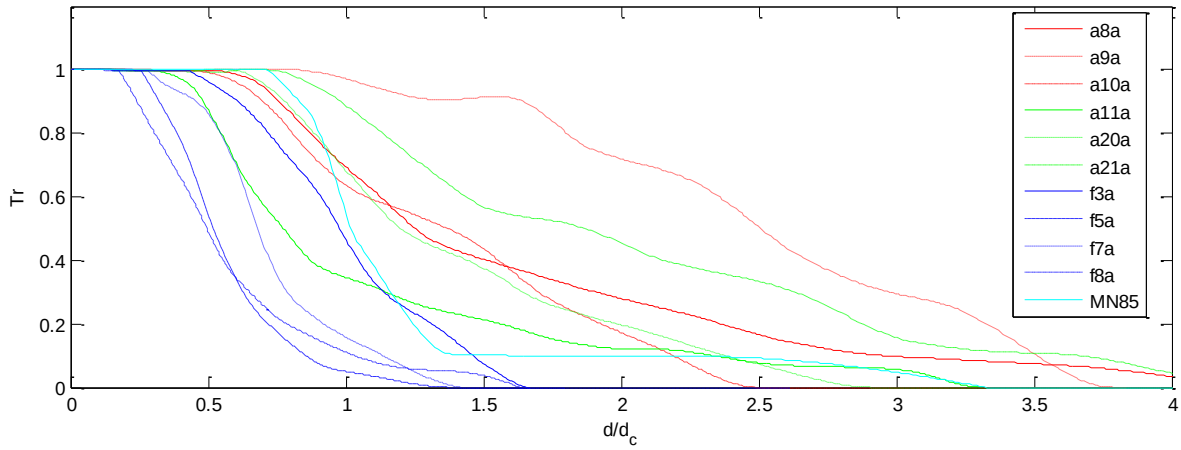

Figure 9. Transfer function Tr plotted against normalised sediment grain diameter for all tests. The normalisation has been carried out using the critical grain diameter d_c in the respective tests (see Table 2).

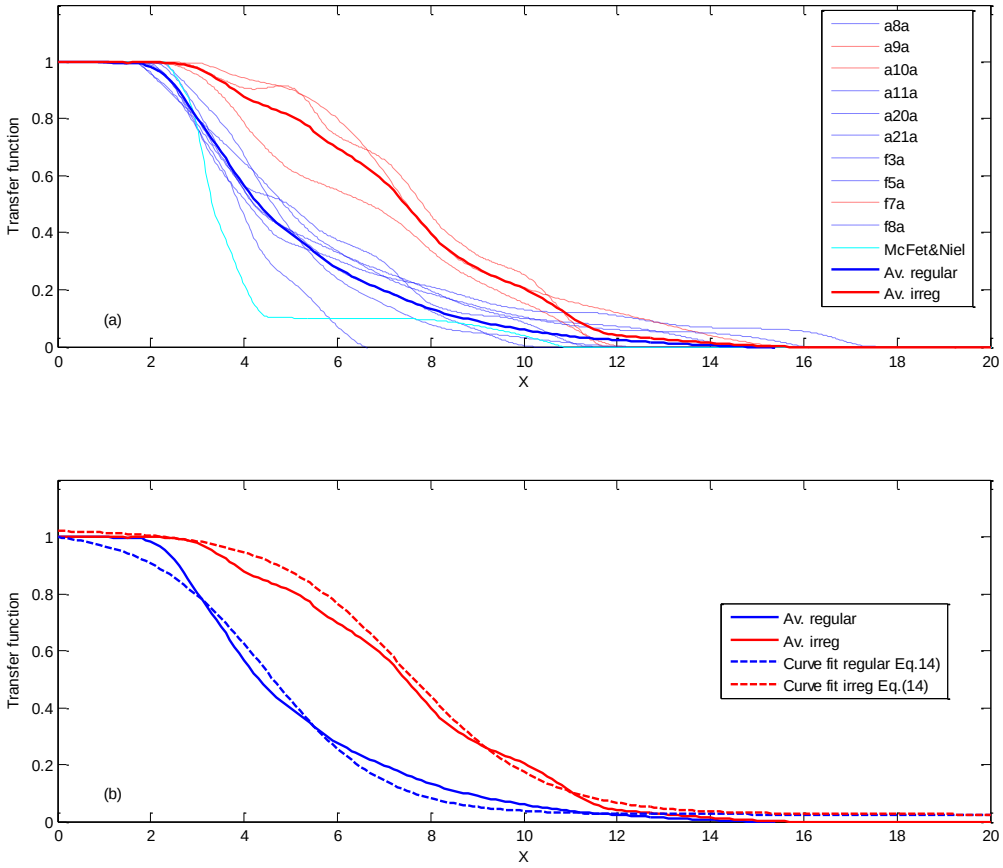

Figure 10. Transfer function plotted against X (see Eq. (14)) Figure a) shows Tr results for all the tests, including that of MN85, with regular wave cases shown as the grouping in blue and the irregular cases in red. Figure a) also includes as full bold curves the average values of the respective blue and red groupings. Figure b) repeats these averaged curves and includes a simple characterisation of each given by Eq. (14) (dashed blue and red bold curves, respectively).

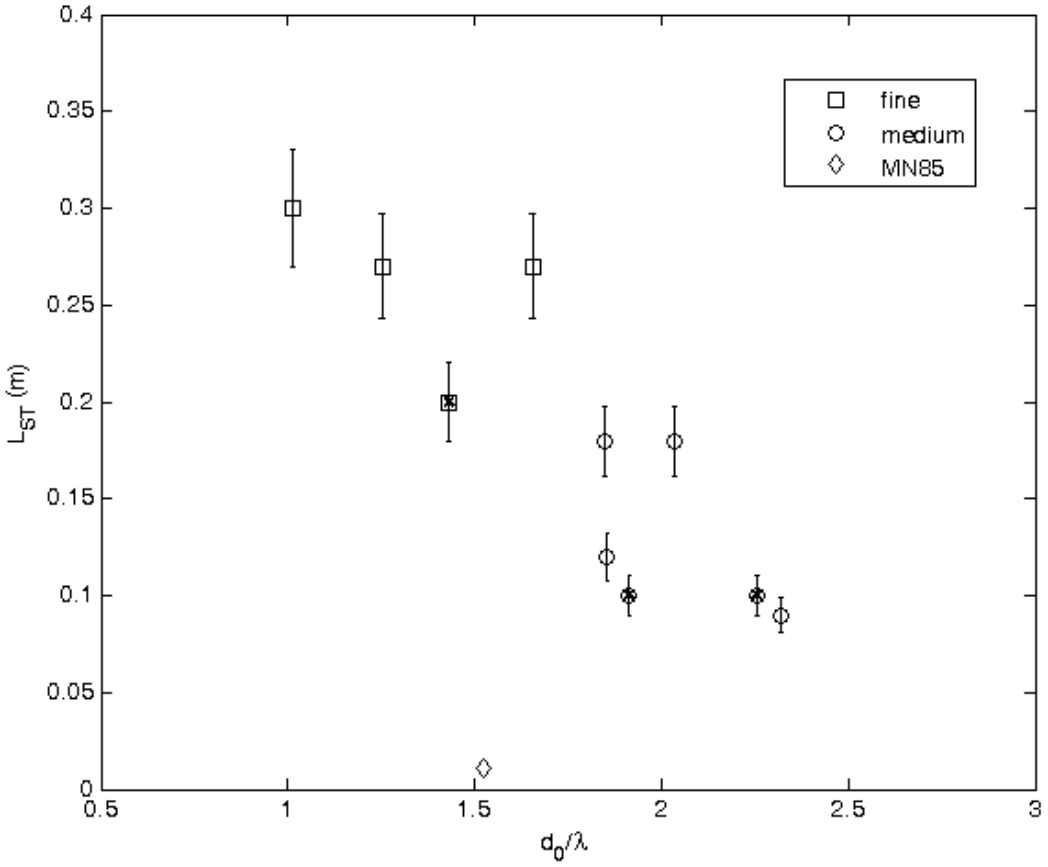

Figure 11. Decay length scale L_{ST} (m) for the total aggregated C- profiles (i.e. comprising the sum of all the grain fractions) for each test plotted against the quotient of near-bed orbital diameter d_0 and ripple wavelength λ. The fine and medium sand cases from the Deltaflume, with standard deviation error included, are shown by the symbols □ and O, respectively, and the result of MN85 by the symbol ◊. The Deltaflume cases involving irregular waves (JONSWAP spectrum) are shown by a cross superimposed on the respective symbols.

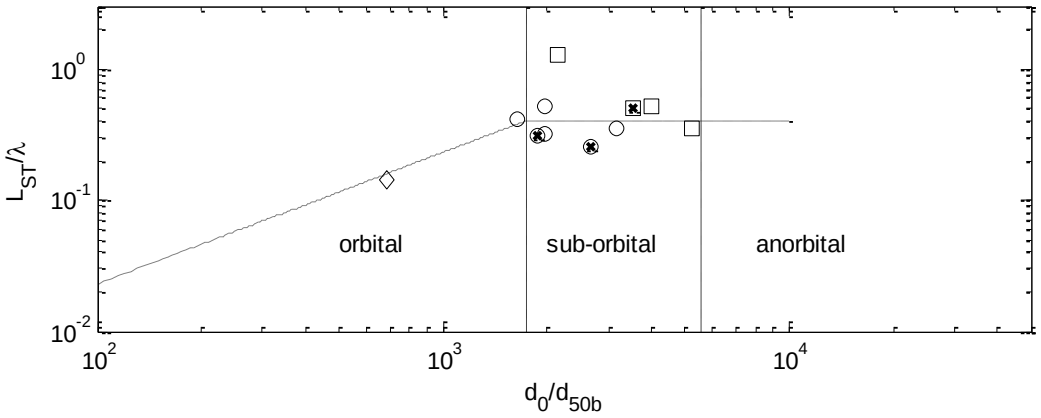

Figure 12. Total decay length scale L_{ST} scaled by ripple wavelength λ and plotted for comparison with the ripple dimensions shown in Figure 3. The orbital, sub-orbital and anorbital ripple ranges of Wiberg and Harris (1994) are as indicated. The dashed line suggests a behaviour for L_{ST}/λ that is constant (=0.4) in the sub-orbital range and, tentatively, linearly increasing towards this value in the orbital range. The symbols are the same as those used in Figure 11, including the crosses indicating the irregular wave cases.

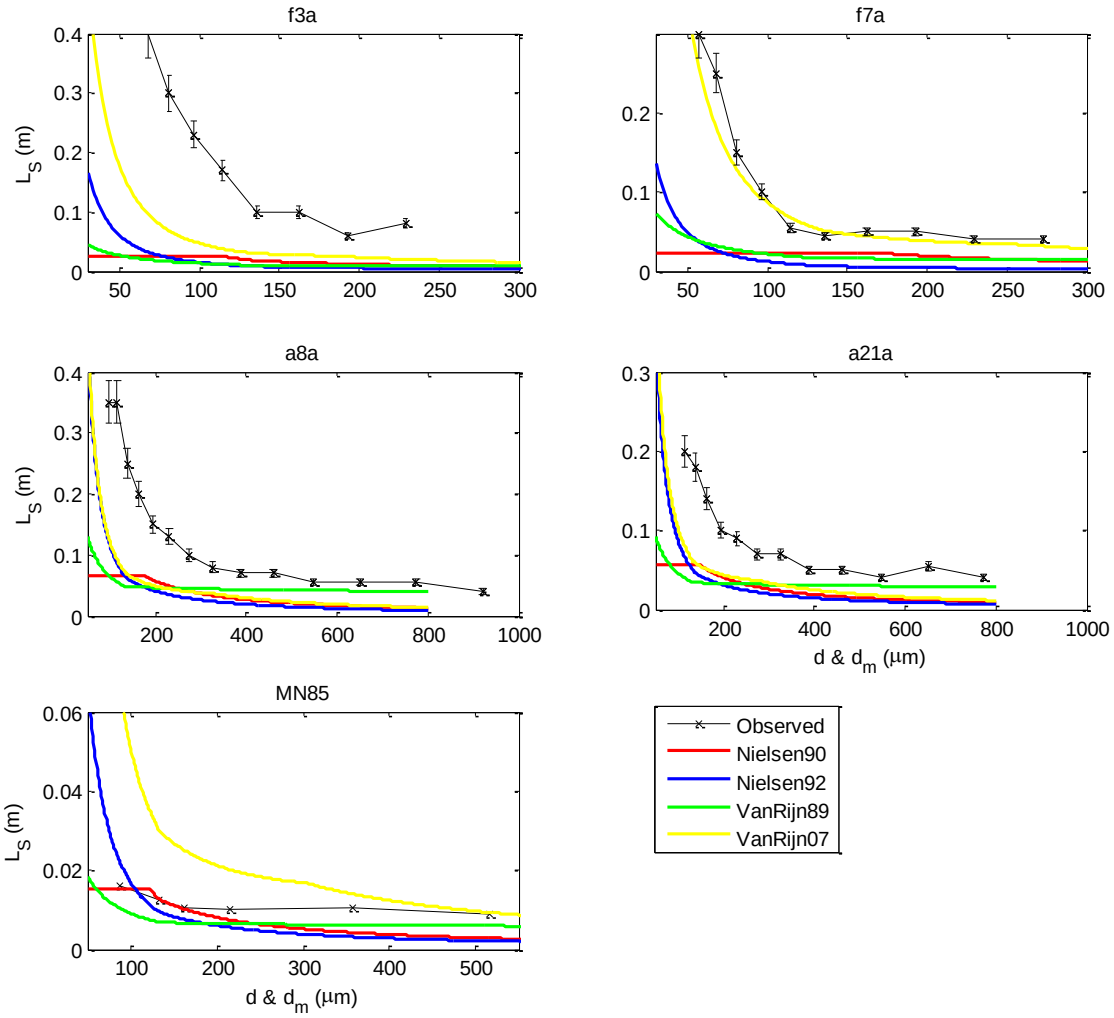

Figure 13. Decay scales L_S (m) (full black lines) determined from exponential curve fitting for each grain fraction (c.f. Eq.(5)) in two typical Deltaflume tests with fine sand (f3a and f7a) and two tests with medium sand (a8a and a21a). Also shown are the L_S values determined by MN85 for their laboratory experiment. In each subplot, where the data are concerned grain diameter d_m denotes the central diameter for each sieve interval. Also plotted as continuous functions of grain diameter d are four formulations for L_S due to i) Nielsen (1990) (Eq.(11)), ii) Nielsen (1992) (Eqs. (2) and (3)), iii) Van Rijn (1989) (Eq.(9)), and iv) Van Rijn (2007a) based on a modified Eq. (9).

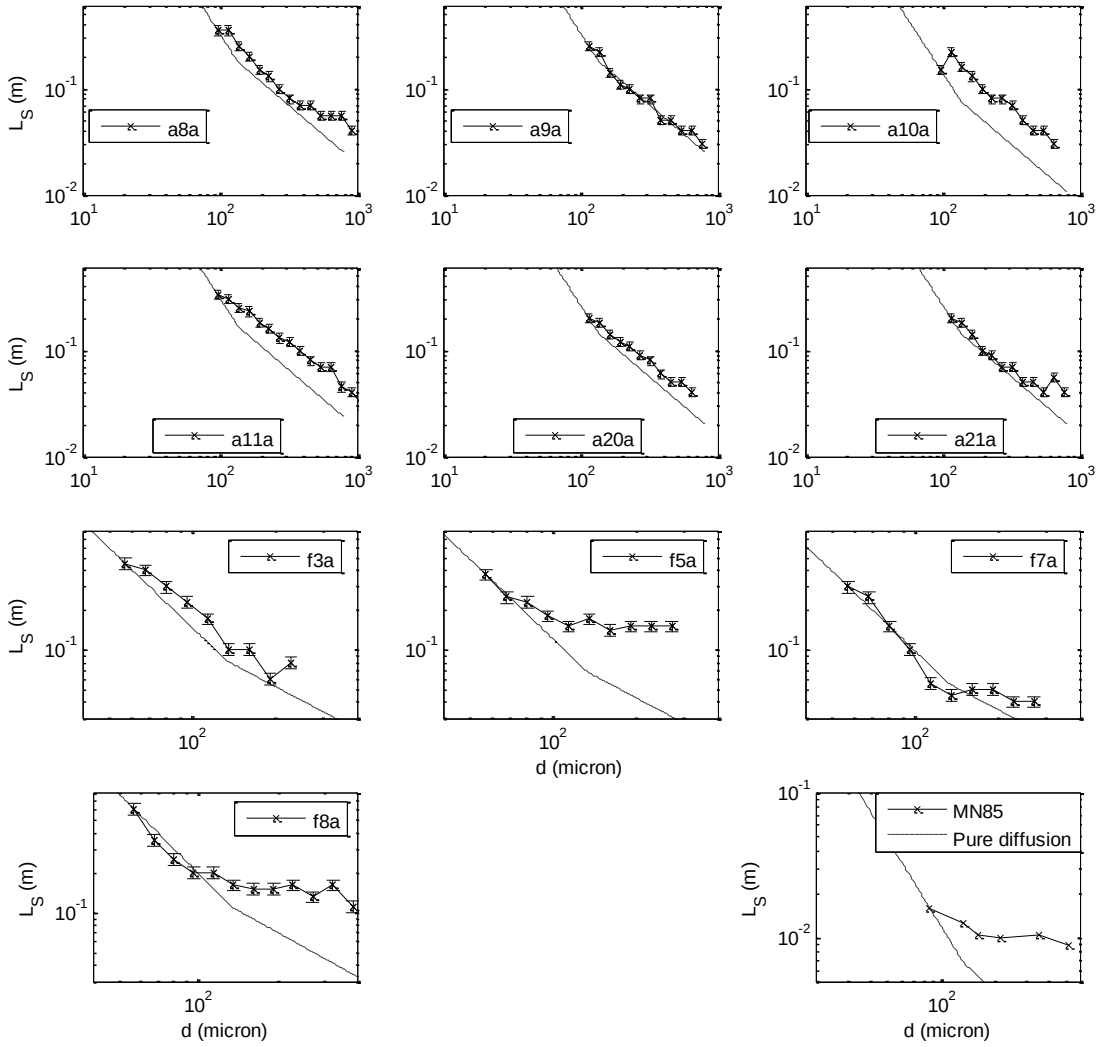

Figure 14. Decay scales L_S (m) obtained for each test (full lines with symbols) in comparison with scaled 'pure diffusion' (dashed) curves for L_S ($=\varepsilon_s/w_s$) arising from Nielsen's (1992) expression for the sediment diffusivity ε_s (Eqs.(2) ad (3)) together with Hallermeier's (1980) formulation for the settling velocity w_s. In each subplot the 'pure diffusion' expression has been scaled to match the observed value of L_S for the smallest grain fraction.

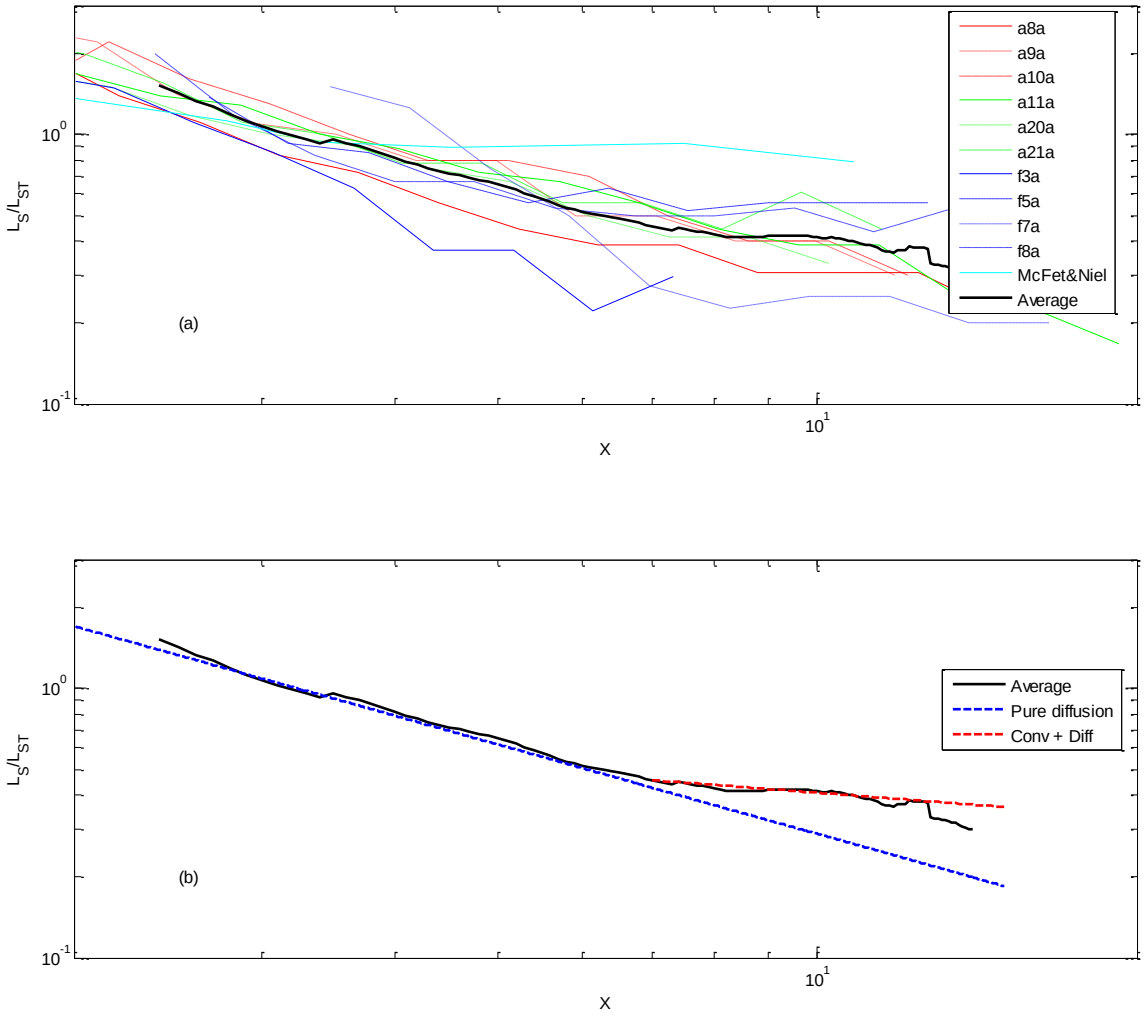

Figure 15. Normalised decay scale L_S plotted against X. Figure a) shows results for all the Deltaflume tests together with the average behaviour of L_S/ L_{ST} which is indicated by the full black line. Also included is the laboratory test of MN85. Figure b) repeats the average curve for L_S/ L_{ST} and adds a two- part, power law, characterisation showing a 'diffusive' behaviour for X<7 and a combined 'convective + diffusive' behaviour for X>7.

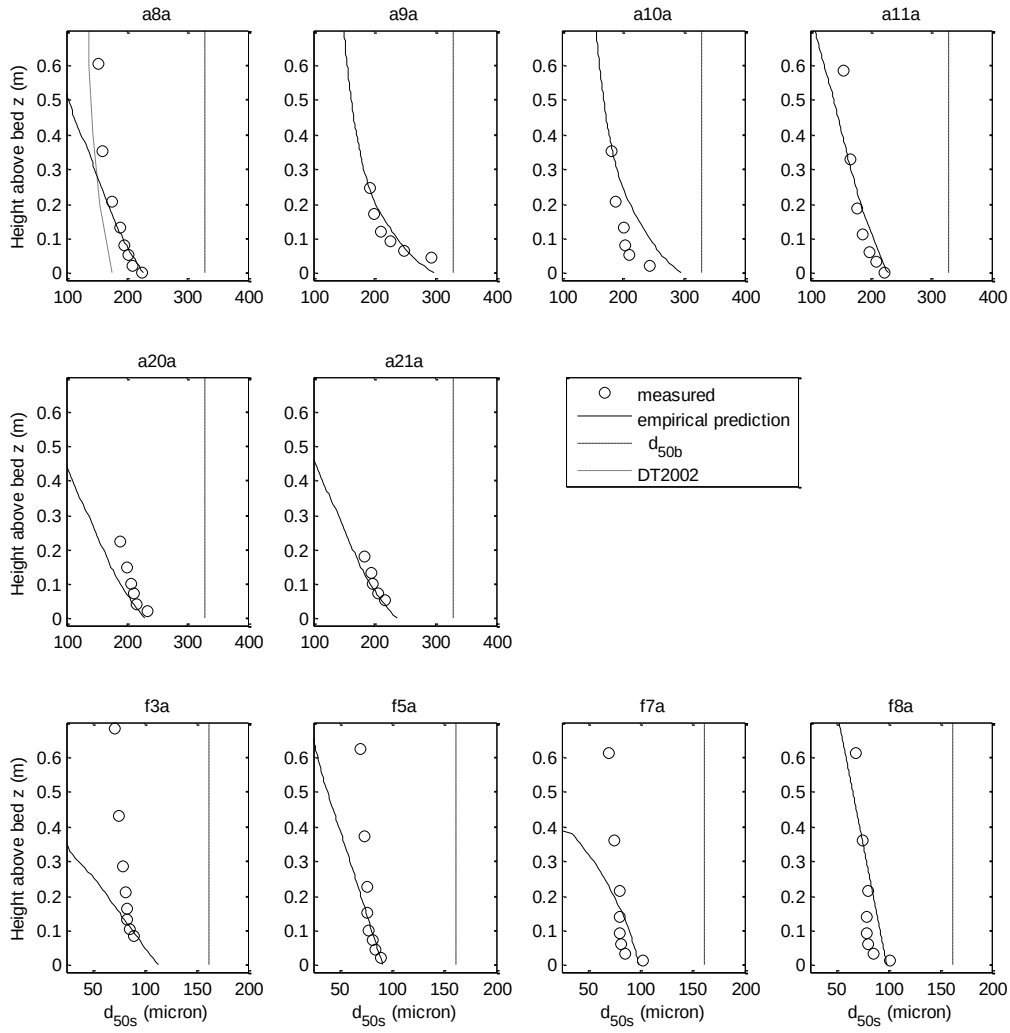

Figure 16. Vertical profiles of d_{50s} the median diameter of the suspended sediment in each Deltaflume test. The symbols (o) indicate the measured values of d_{50s} and the dashed lines indicate the median diameter of the respective bed sediment d_{50b}. The predicted empirical fit (full lines) in each subplot is based on i) the cumulative size distribution for the bed sediment (Fig. 1), ii) the Transfer function (Eq. (13)) defined according to the distinction made in Eq. (14) between regular and irregular waves (see Fig. 10) and iii) the decay length scale relationship given by Eq. (17). In the subplot for test a8a, the black dotted line reproduces the d_{50s} profile presented for this case by Davies and Thorne (2002) [DT2002].

Appendix A

C-profile for constant + linear diffusivity

Thorne et al. (2002) compared total C-profiles (i.e. the sum of all fractions), obtained using an acoustic backscatter system, ABS, in the Deltaflume, above the medium sand bed with Nielsen's (1992) 'convection-diffusion' and 'pure convection' profiles. The latter solution, which is of power law type, arises from consideration of the probability of a particle being entrained to a defined height above the bed. They found that both profile types could be tuned to give good agreement with the ABS data and considered the sediment diffusivity profile that was implied by treating the 'pure convection' profile as a solution of the sediment diffusion equation. The resulting sediment diffusivity profile turned out to have a 'constant + linear' nature. In a model intercomparison with C-profile data, such a profile was found by Sistermans (2002) to be both the optimum one for waves + current above a rippled bed and also as good as a height-constant profile for waves alone above ripples. A critical consideration in each case was that, in the rippled regime, the ε_s profile should <u>not</u> tend to zero on approaching the bed.

The analysis in the present paper has focussed on interpretations involving a height-constant sediment diffusivity ε_s and the corresponding exponential C-profile shape. At the same time it has been apparent that a minority of the individual C-profiles (for individual fractions within a test) are better described by a linearly height-varying diffusivity corresponding to a power law profile. With the steady state diffusion equation given by Eq.(1):

$$\varepsilon_s \frac{dC}{dz} + w_s C = 0 \tag{A.1}$$

it is potentially relevant therefore to consider a sediment diffusivity having the assumed form:

$$\varepsilon_s = a + bz \tag{A.2}$$

where parameters a and b are independent of height z above the bed. [As noted in §1, for rippled and very rough beds in a wave-induced flow, it can be assumed that, e.g., $a = 0.016 U_1 k_s$, $b = 0$ and, for flat rough beds, e.g., $a = 0$, $b = \kappa u_{*w}$.]

The solution of Eq.(A.1) subject to (A.2) is simply:

$$C = (a + bz)^{-w_s/b} + constant \tag{A.3}$$

and, taking the boundary condition $C=C_r$ at $z=z_r$ it follows that:

$$\frac{C}{C_r} = \left(\frac{a+bz_r}{a+bz}\right)^{w_s/b} \tag{A.4}$$

This solution reverts to the usual Rouse-type power law (c.f. Eq.(7)) in the limit $a \rightarrow 0$:

$$\frac{c}{c_r} = \left(\frac{z_r}{z}\right)^{w_S/b} \tag{A.5}$$

while, in the limit b→0, an exponential profile (c.f. Eq.(5)) is recovered, the formal limiting process being more involved in this case:

$$C = C_r e^{-z/L_S} \tag{A.6}$$

where $L_S = a/w_s$.

In a simple schematised way, one can illustrate the change from a power law to exponential law C-profile by changing the ratio a:b. In the illustrative example in Figure A.1, a=[0 0.4 1 2.5] and b=[5 2 1 0.5] giving the 4 (dimensional) quotients a/b shown in the legend, together with the exponential profile case for which a/b is infinite. Figure A.1a shows a linear plot of the 5 profiles each of which takes value unity at the level z_{ref}. The same curves are plotted in Figure A.1b in a log-log plot. The power law (a/b=0) becomes a straight line while other curves for non-zero values 'a' of become strongly curved. In Figure A.1c the curves are next plotted using log-linear axes. Now the exponential curve (a/b=∞) is a straight line, while the remaining curves become curved in the opposite sense. It is evident that fairly straight lines are found in this plot for the wide range of values having a/b > 1. This latter point might help to explain why the exponential fitting method works well for most of the C-profile fractions in most of the tests in the Deltaflume, and why Sistermans (2002) found that several different possible functional forms for ε_s that he considered gave roughly similar C-profile shapes.

Appendix B

Nielsen's (1992) 'selective entrainment' concept interpreted as a Transfer function

As noted in §2.1 Nielsen (1992, §5.3.7) commented on the lack of information available about the selective entrainment of different sand sizes under waves and suggested the simple formula:

$$\frac{fraction\ in\ bed}{fraction\ in\ near\ bed\ suspension} \approx \frac{d}{d_{50b}} \tag{B.1}$$

This approach, which is included for comparison in Figure 6, was based on a limited amount of graded-sediment data obtained for the *very rough / rippled* turbulent regime ~~rippled beds under waves~~, including both field data (RE=(2.6-5.0)×10^5, A_1/k_s=1.7-3.5, see Nielsen, 1983) and also the laboratory data of MN85 (RE=0.11×10^5, A_1/k_s=1.5). In practice, the linear dependence on d/d_{50b} of the quotient on the left hand side of Eq.(B.1) will only provide a reasonable description of the

entrainment process up to the point where the sediment capable of being put into suspension is exhausted. A departure from the linear dependence necessarily then occurs, as is evident in Nielsen's (1992) Figure 5.3.6 for the largest grain fraction in the experiment of MN85. For the Deltaflume tests a pronounced departure from the linear behaviour occurs for $d/d_{50b} \geq 1$ for the fine sand and $\geq$ 1.5 for the medium sand (figure not shown). Figure B.1 shows the Transfer functions, defined by Eq. (13), consequent upon the use of Eq.(B.1) for both the fine and medium sand bed distributions in the Deltaflume and also for the fine sand used in the experiment of MN85. The functional form for Tr in each case is qualitatively similar to the results plotted in Figure 8, but the variation exhibited by the individual tests in each group is absent. More importantly, the magnitudes of the Transfer functions based on the selective entrainment argument become progressively larger than observed as d/d_{50b} increases, as a result of the breakdown of Eq.(B.1) for the larger fractions. This bias is seen for all of the Deltaflume tests and also for the test of MN85 for which the observed Tr values in Figure 8 are ~0.1 for the largest fractions, but are ~0.3 from use of Eq.(B.1). The preference in the present paper for the use of the functional form for Tr given by Eq.(13), rather than a form like Eq.(B.1) or a fractional reference concentration approach, arises from both the limitations of the latter equation and also the present emphasis on the behaviour of the coarser fractions which is best analysed using a description like Eq.(13)

Appendix C

Hallermeier's (1981) settling velocity formulation

The formulation is expressed here for a single natural sand grain of diameter d settling in still water, rather than as the median diameter in Hallermeier's paper. The Reynolds number of the settling grain is given by

$$\mathrm{Re}_s = \frac{w_s d}{\nu} \tag{C.1}$$

and the Archimedes Buoyancy Index, which is related to the dimensionless grain size D_*, by:

$$A_* = D_*^3 = \left(\frac{\rho_s - \rho}{\rho} \right) \frac{g d^3}{\nu^2} \tag{C.2}$$

where ν = kinematic viscosity, g = acceleration due to gravity and ρ_s, ρ = sediment, fluid density.

The settling velocity w_s is obtained from the following equations for the respective regimes:

$$\mathrm{Re}_s = \frac{w_s d}{\nu} = \begin{cases} A_*/18 & for \quad A_* < 39 & [Stokes\ regime] \\ A_*^{0.7}/6 & for \quad 39 < A_* < 10^4 & [Transitional\ regime] \\ 1.05 A_*^{0.5} & for \quad 10^4 < A_* < 10^6 & [Turbulent\ regime] \end{cases} \qquad (C.3)$$

For natural sand grains settling in fresh water (ρ_s/ρ=2.65, ν=1 mm^2/s, g=9810 mm/s^2) the transitional regime corresponds to the grain size range [134,851] micron.

Appendix D

Determination of the profile of the median diameter of the suspended sediment d_{50s}

The method used in §7 involved the following steps for each test:

1. The appropriate bed sediment size distribution in Figure 1 was interpolated using 100 intervals of 10 μm for the medium sand and 5 μm for the fine sand. The grain diameter attributed to each interval was the central size for that interval.
2. The Transfer function (Eq.(14)) was used to convert the bed size distribution into a cumulative distribution for the reference concentration using the 100 defined grain size intervals. The ripple dimensions (η,λ) were taken from Table 1, together with the appropriate value of d_{50b} and coefficients (b_1,b_2) appropriate for regular/irregular waves for use in Eq.(14).
3. The cumulative reference concentration curve was discretized into individual reference concentration values corresponding to the 100 grain size intervals.
4. The total decay length scale L_{ST} was determined based on the scheme shown in Figure 12.
5. For each grain size d the value of decay scale L_S was determined using Eq.(17) with coefficient c_4 defined according to the value of X.
6. Using the set of reference concentrations and corresponding L_S values, concentration profiles $C_i(z_j)$ were determined for each of the 100 grain sizes (i) at a set of 100 heights (j) above the crest, from z = 0 to 1m with an interval of 0.01m.
7. At each height j, the 100 concentration values for each test were summed to give the total concentration $C_{sum}(z_j)$.
8. The cumulative concentration $C_{cum,i}(z_j)$ at each height z_j was determined and normalised by the value $C_{sum}(z_j)$.

9. Finally, from the resulting quotient $C_{cum,i}(z_j)/C_{sum}(z_j)$ the values of $d_{50s}(z_j)$ were determined by interpolation among the sizes to yield the '50% finer than' size value.

Figures : Appendices

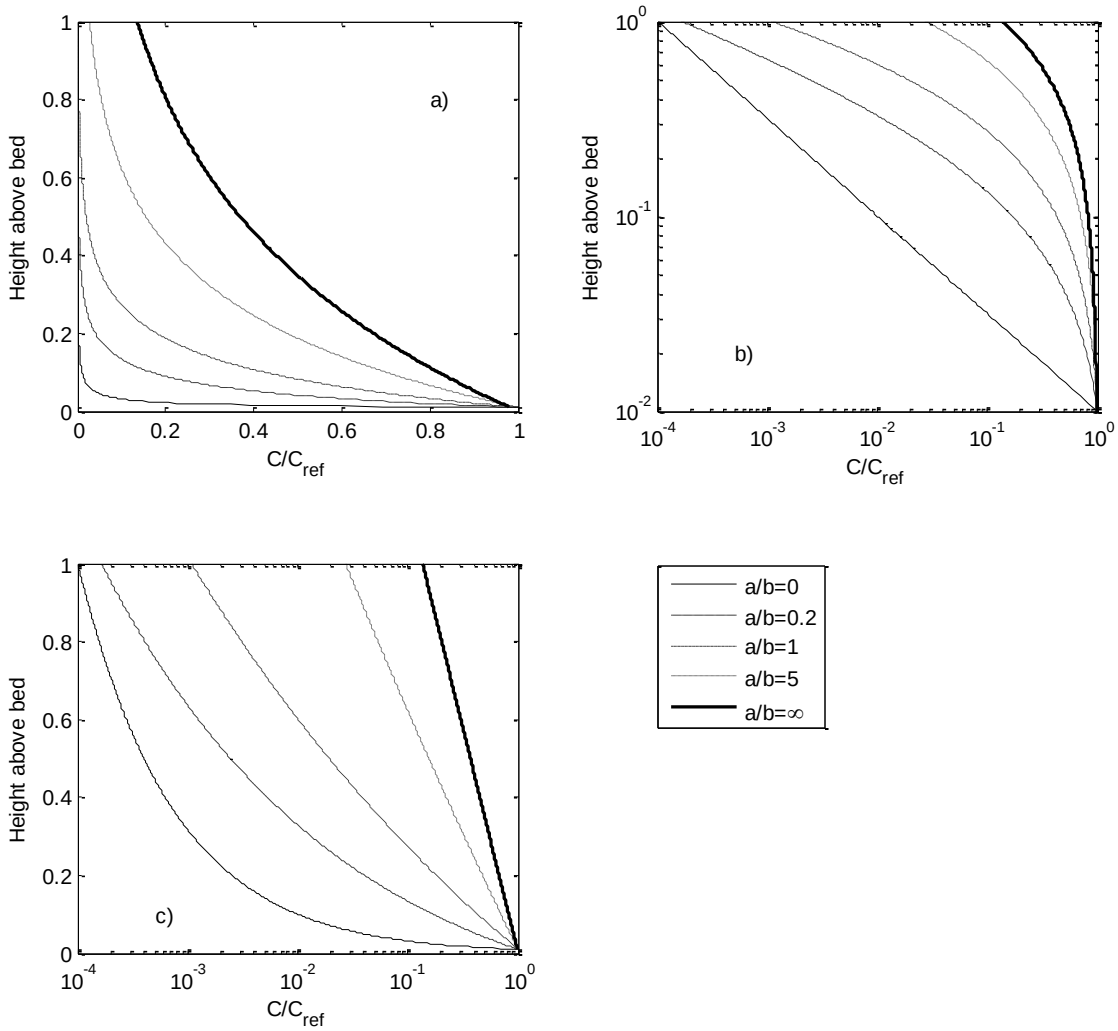

Figure A.1. Schematisation of C-profiles based on Eq.(A.4) for a range of values of the (dimensional) quotient a/b.

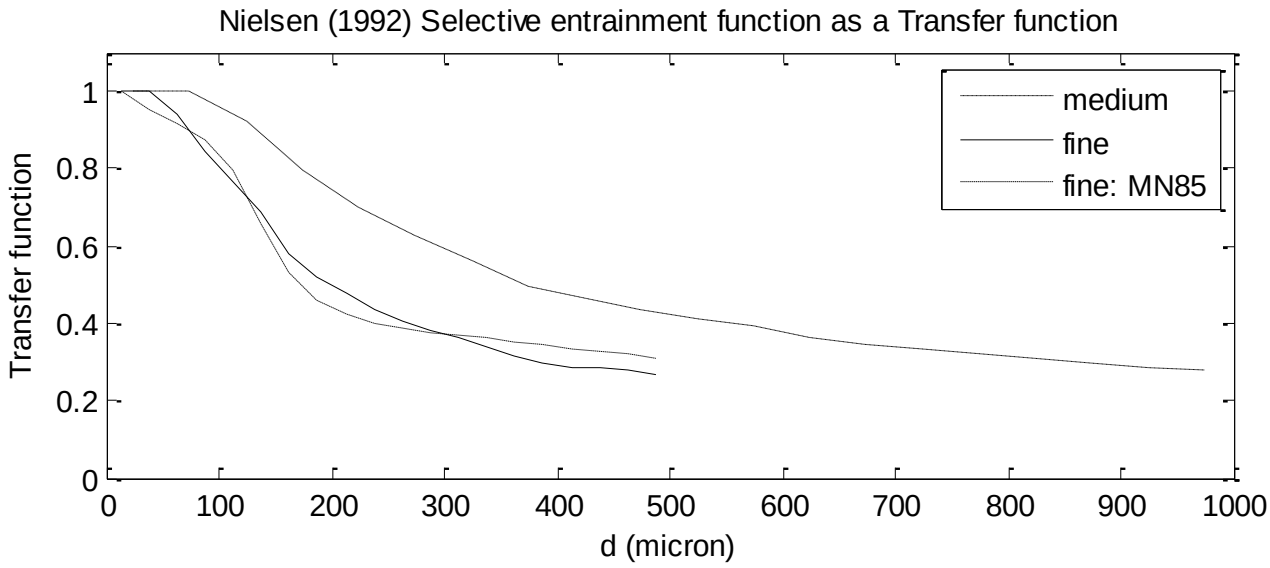

Figure B.1. Transfer functions calculated on the basis of Nielsen's (1992) 'selective entrainment' function (Eq.(B.1)) for the fine and medium sand beds in the Deltaflume and also the fine sand bed used in the experiment of MN85. The calculations have been made by i) converting the cumulative bed grain size distributions shown in Figure 1 into 20 separate fractions, ii) applying Eq.(B.1) to each fraction, iii) calculating the resulting cumulative size distributions of the reference concentration (c.f. Figure 7), and iv) using Eq.(13) to determine the respective Transfer functions shown in this figure. While the results are qualitatively similar to those in Figure 8, they do not discriminate between different test conditions and, importantly, exhibit bias to relatively larger Tr values than observed, particularly for the larger grain fractions within each Deltaflume grouping.